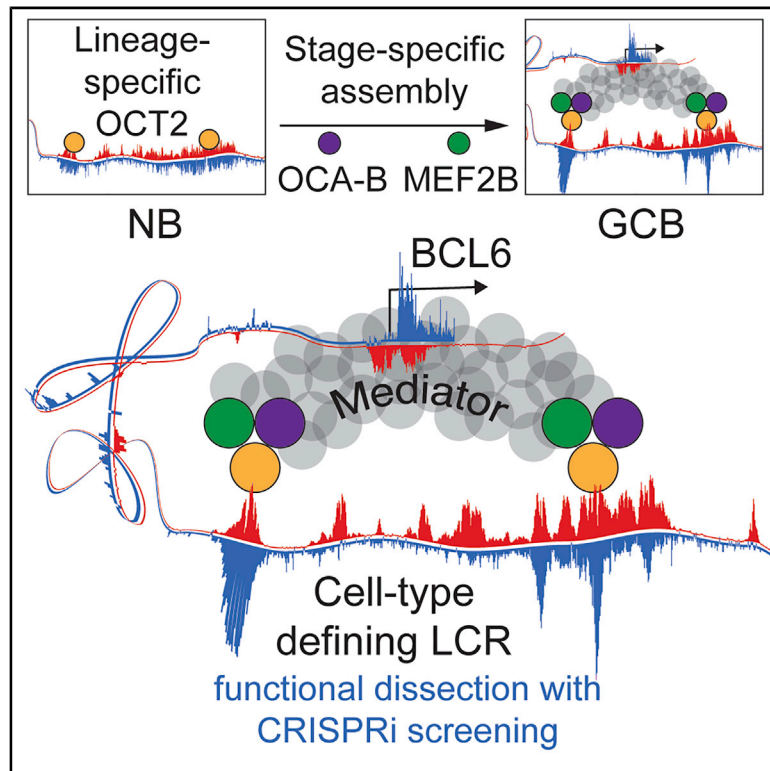


# Unique Immune Cell Coactivators Specify Locus Control Region Function and Cell Stage

## Graphical Abstract



## Authors

Chi-Shuen Chu, Johannes C. Hellmuth, Rajat Singh, ..., Olivier Elemento, Ari M. Melnick, Robert G. Roeder

## Correspondence

amm2014@med.cornell.edu (A.M.M.), roeder@rockefeller.edu (R.G.R.)

## In Brief

Chu and Hellmuth et al. reveal hierarchical regulation involving a ternary transcriptional complex, OCT2·OCA-B·MEF2B, composed of lineage- and stage-specific factors, as a critical component utilizing distinct essential enhancer elements in the LCR, essential for timely induction of *BCL6*, a master regulator for germinal center B cell differentiation.

## Highlights

- OCT2·OCA-B binds heavily across the *BCL6* LCR
- OCT2, OCA-B, and MEF2B form a ternary complex controlling *BCL6* LCR activity
- OCA-B directly recruits Mediator, bridging the *BCL6* LCR to the *BCL6* promoter in *cis*
- Four distinct OCT2·OCA-B·MEF2B-binding enhancers are essential for LCR function

Article

# Unique Immune Cell Coactivators Specify Locus Control Region Function and Cell Stage

Chi-Shuen Chu,<sup>1,7</sup> Johannes C. Hellmuth,<sup>2,6,7</sup> Rajat Singh,<sup>2</sup> Hsia-Yuan Ying,<sup>2</sup> Lucy Skrabanek,<sup>3,4</sup> Matthew R. Teater,<sup>2</sup> Ashley S. Doane,<sup>2,3</sup> Olivier Elemento,<sup>3,5</sup> Ari M. Melnick,<sup>2,\*</sup> and Robert G. Roeder<sup>1,8,\*</sup>

<sup>1</sup>Laboratory of Biochemistry and Molecular Biology, The Rockefeller University, New York, NY 10065, USA

<sup>2</sup>Department of Medicine, Division of Hematology & Medical Oncology, Weill Cornell Medicine, New York, NY 10065, USA

<sup>3</sup>Department of Physiology and Biophysics, Institute for Computational Biomedicine, Weill Cornell Medicine, New York, NY 10065, USA

<sup>4</sup>Applied Bioinformatics Core, Weill Cornell Medicine, New York, NY 10065, USA

<sup>5</sup>Caryl and Israel Englander Institute for Precision Medicine, Weill Cornell Medicine, New York, NY 10065, USA

<sup>6</sup>Present address: Department of Medicine III, University Hospital, LMU, Munich 81377, Germany

<sup>7</sup>These authors contributed equally, alphabetically ordered

<sup>8</sup>Lead Contact

\*Correspondence: [amm2014@med.cornell.edu](mailto:amm2014@med.cornell.edu) (A.M.M.), [roeder@rockefeller.edu](mailto:roeder@rockefeller.edu) (R.G.R.)

<https://doi.org/10.1016/j.molcel.2020.10.036>

## SUMMARY

Locus control region (LCR) functions define cellular identity and have critical roles in diseases such as cancer, although the hierarchy of structural components and associated factors that drive functionality are incompletely understood. Here we show that OCA-B, a B cell-specific coactivator essential for germinal center (GC) formation, forms a ternary complex with the lymphoid-enriched OCT2 and GC-specific MEF2B transcription factors and that this complex occupies and activates an LCR that regulates the *BCL6* proto-oncogene and is uniquely required by normal and malignant GC B cells. Mechanistically, through OCA-B-MED1 interactions, this complex is required for Mediator association with the *BCL6* promoter. Densely tiled CRISPRi screening indicates that only LCR segments heavily bound by this ternary complex are essential for its function. Our results demonstrate how an intimately linked complex of lineage- and stage-specific factors converges on specific and highly essential enhancer elements to drive the function of a cell-type-defining LCR.

## INTRODUCTION

During the humoral immune response, subsets of activated B cells form transient structures called germinal centers (GCs), where they manifest a unique proliferative phenotype tolerant of genomic instability to facilitate immunoglobulin affinity maturation (Mesin et al., 2016). Entry into the GC reaction requires B cells to undergo profound epigenetic and transcriptional reprogramming that involves repression of many immune signaling and checkpoint genes by *BCL6*, a transcriptional repressor highly induced in and essential for formation of GC B cells (Mlynarczyk et al., 2019). Although *BCL6* is an essential master regulator of the GC reaction (Dent et al., 1997; Fukuda et al., 1997; Ye et al., 1997), the mechanism through which its expression is induced and maintained in GC B cells remains poorly understood. Defining how GC stage-specific *BCL6* expression is achieved is critical for understanding not only GC B cells but also the diffuse large B cell lymphomas (DLBCLs) and follicular lymphomas (FLs) that arise from GC B cells and are dependent on sustained expression of *BCL6* for their survival (Basso and Dalla-Favera, 2015). The *BCL6* requirement for formation of

GC B cells illustrates how specific cell lineages are dependent on particular transcription factors (TFs) to elicit their phenotype.

Gene-specific functions of TFs are mediated through interactions with non-coding regulatory regions of the genome. In this regard, genome-wide high-throughput chromosome conformation capture (Hi-C) studies in primary B cell populations revealed a GC-specific intergenic region, located 150 kb upstream of *BCL6* on chromosome 3q26, that has been suggested to function as a locus control region (LCR) through extensive interactions with neighboring and distal genes that include *BCL6* (Bunting et al., 2016). This large region, spanning more than 100 kb, also has super enhancer characteristics based on acetylation of histone H3 on lysine 27 (H3K27ac) or BRD4 chromatin immunoprecipitation sequencing (ChIP-seq) data in GC-derived lymphoma cells (Ramachandradevdy et al., 2010; Chapuy et al., 2013; Ryan et al., 2015). In contrast to the early lethality caused by defects in non-B cells in *Bcl6*<sup>-/-</sup> mice, constitutive deletion of the *Bcl6* LCR yields generally healthy animals that, nonetheless, are completely unable to form GCs (Bunting et al., 2016), indicating that the function of the LCR is GC-specific and essential for GC formation. Based on DNase I hypersensitive sites, this

large LCR contains numerous putative regulatory elements (TF binding sites) whose individual contributions to LCR function and GC biology are unknown. In fact, no enhancer element has been functionally defined as being required for *BCL6* expression, and the mechanisms underlying the function of such elements as lineage specification determinants are not well understood.

OCA-B is the first factor shown to be essential and selective for GC formation (Schubart et al., 1996; Nielsen et al., 1996; Kim et al., 1996). Otherwise healthy *Pou2af1*<sup>-/-</sup> (gene name for OCA-B) mice have been found to be completely deficient in GC formation, as found later in *Bcl6* and *Bcl6* LCR deletion mice. Like *BCL6*, OCA-B has also been implicated in growth of GC-derived DLBCL cells (Chapuy et al., 2013). OCA-B was initially identified as a B cell-specific coactivator that can facilitate transcription from immunoglobulin (*Ig*) gene promoters through interactions with either the ubiquitous (OCT1) or the lymphoid lineage (OCT2) octamer-binding TF (Luo et al., 1992; Luo and Roeder, 1995) and has been shown to facilitate transcription from *Ig* enhancers in cell-based assays (Stevens et al., 2000). Apart from the *Ig* locus, other genes, including *Cxcr5*, *Cd79a*, *Cd79b*, *Kcnn4*, *Lck*, *SpiB*, and *miR-146a*, are thought to be directly regulated by OCA-B under various conditions in mouse splenic B cells or cell lines (Wolf et al., 1998; Malone and Wall, 2002; Kim et al., 2003; Bartholdy et al., 2006; Lindner et al., 2014). Genes involved in broad B cell programs have been proposed as OCA-B targets in response to OCT2 knockdown in activated B cell (ABC) DLBCLs (Hodson et al., 2016). However, unlike *Bcl6* or *Bcl6* LCR deletion, deletion of the abovementioned genes does not have effects that resemble the GC defects of *Pou2af1* deletion. Furthermore, to date, there has been no comprehensive understanding of direct OCA-B target genes or mechanistic aspects of OCA-B coactivation functions in relation to its essential role in GC formation.

Along these lines, complementary analyses of (1) direct target genes of OCA-B and its mechanism of action and (2) key regulatory elements and associated factors in the *BCL6* LCR led us to propose that OCA-B directly regulates *BCL6* expression in GC B cells. Using genomic and biochemical approaches, we uncover (1) a previously uncharacterized ternary complex composed of OCT2, OCA-B, and the GC-specific TF MEF2B and (2) its function in the *BCL6* LCR through facilitation of Mediator recruitment and enhancer-promoter looping. Densely tiled clustered regularly interspaced short palindromic repeats interference (CRISPRi) screening indicates that only LCR segments heavily bound by this ternary complex are essential for LCR function. Our results indicate a multi-tiered cooperativity that precisely defines the enhancer specificity and function of a master developmental regulator.

## RESULTS

### OCA-B and OCT2 Are Highly Enriched at the *BCL6* LCR

Based on the high GC expression of OCA-B and *BCL6* and the GC defect in *Pou2af1*<sup>-/-</sup> and *Bcl6*<sup>-/-</sup> mice, we reasoned that OCA-B might control the *BCL6* LCR. An investigation of genome-wide binding patterns of OCA-B, OCT1, and OCT2 in the GC-derived DLBCL line OCI-Ly7 by ChIP-seq showed a more prominent overlap of OCA-B with OCT2 (75.7%) than

with OCT1 (32.1%) (Figures 1A and S1A). Over 35% of the OCA-B or OCT2 peaks were located in intergenic or intronic enhancer regions (Figure 1B). In this group, OCA-B and OCT2 ChIP-seq signals were highly enriched at active enhancers relative to primed enhancers and enriched more dramatically at super enhancers (Figures 1C and S1B–S1D; Lovén et al., 2013; Whyte et al., 2013). *De novo* motif analyses of OCT2 and OCA-B binding sites revealed enrichment for the canonical OCT2 motif, as expected, as well as motifs for B cell-related ETS family TFs (SPIB, PU.1, and ETS) and genome architectural factors (CTCF and its homolog BORIS) (Figure 1D). The Rank Ordering of Super-Enhancers (ROSE) algorithm also identified the *BCL6* LCR as one of the most enriched genomic regions for OCA-B and OCT2 (Figure 1E). Subsequent alignment of OCA-B and OCT2 ChIP-seq data with H3K27ac ChIP-seq from human tonsillar naive B and GC B cells and ChIP-seq data for other GC B cell TFs (MEF2B, PAX5, and PU.1) and cofactors (p300, CREBBP, MED1) in OCI-Ly7 cells showed that the majority of these factors/marks were enriched at many of the *BCL6*-LCR constituent enhancers defined by DNase I hypersensitive sites (Figure 1F). Reanalysis of public Blueprint expression data further revealed that, among these factors, expression of OCA-B is highly GC-specific, whereas OCT2 is expressed throughout naive B and GC B cells, in agreement with its role as a B cell lineage-determining TF (Figure 1F). These data point to OCT2 and OCA-B as putative critical functional determinants of the 3q26 *BCL6* LCR required for formation of GC B cells.

### OCA-B Binds to MEF2B to Drive *BCL6* LCR Activity

As further evidence that OCA-B and OCT2 are required to drive *BCL6* expression in GC-derived B cells (OCI-Ly7 cells), CRISPRi-mediated knockdown using two different guide RNAs (gRNAs) each resulted in a marked reduction of *BCL6* mRNA levels (Figure 2A). Similarly, CRISPR-mediated deletion of OCA-B or OCT2 in the same cells yielded markedly reduced *BCL6* protein levels (Figure 2B). To help define the mechanism of action of OCA-B in the context of GC-derived B cells, we performed immunoprecipitation-mass spectrometry (IP-MS) using an anti-OCA-B antibody with OCI-Ly7 cells. Strikingly, we detected a highly significant association of OCA-B with most of the ~30 subunits of the Mediator transcriptional coactivator complex (Malik and Roeder, 2010) and with MEF2B (Figure 2C), another highly GC-specific TF (Figure 1F) whose GC-specific deletion reduces GC formation by ~50% (Brescia et al., 2018). Associations between OCA-B, OCT2, and MEF2B were validated by reciprocal coIP from OCI-Ly7 nuclear extract (Figure 2D). To determine whether these reciprocal associations also reflect the presence of a ternary complex subpopulation, we performed double IP using anti-OCA-B and anti-OCT2 antibodies for the first and second IPs, respectively. Notably, MEF2B was immunoprecipitated in association with the OCT2·OCA-B complex, clearly indicating the existence in OCI-Ly7 cells of a ternary OCT2·OCA-B·MEF2B complex whose formation is independent of DNA binding (Figure 2E). Consistent with previous findings that MEF2B can activate *BCL6* expression (Ying et al., 2013), we observed similar results with both CRISPRi-mediated knockdown (Figure 2F) and CRISPR-mediated deletion (Figure 2G) of MEF2B in OCI-Ly7

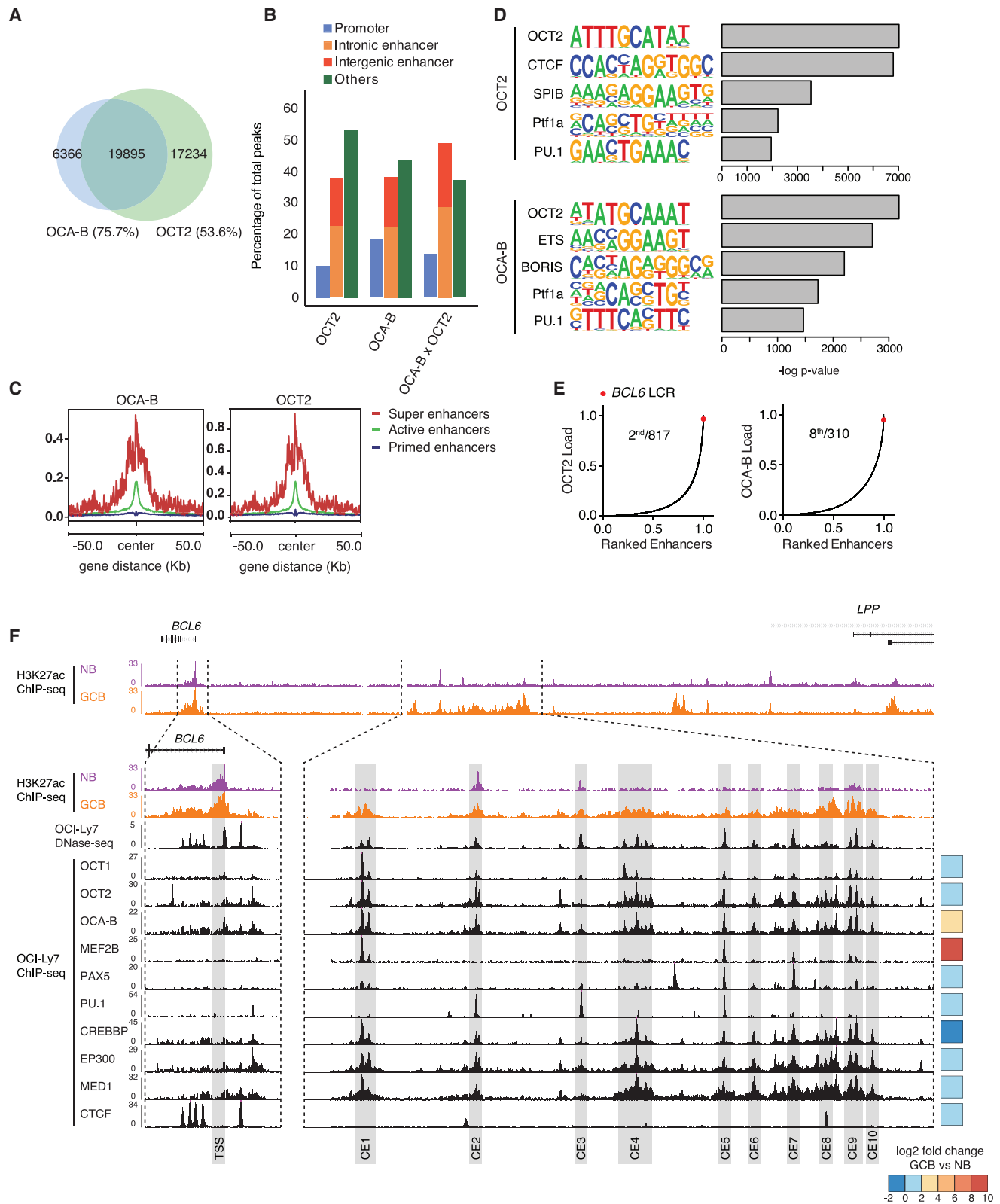


**Figure 1. OCA-B and OCT2 Are Highly Enriched at the *BCL6* LCR**

(A) Overlap of OCT2 and OCA-B ChIP-seq peaks in OCI-Ly7 cells.

(B) Genomic distribution of OCT2 or OCA-B ChIP-seq peaks.

(legend continued on next page)

cells. Although OCT2 and OCA-B expression levels were barely affected by reciprocal knockdown, expression of MEF2B was reduced after OCT2 and OCA-B knockdown (Figure S2A), suggesting more complicated feedback loop-mediated regulation of OCT2·OCA-B on MEF2B for *BCL6* activation.

The high abundance of these three factors at the *BCL6* LCR, comprised of numerous constituent enhancers (Figure 1F), led us to investigate whether they drive *BCL6* enhancer-like functions through direct binding. Although some of the constituent enhancers (e.g., CE2, CE3, and CE9) showed H3K27ac marks and chromatin accessibility as early as the naive B cell stage, the majority (e.g., CE1, CE4, and CE7) were GC-specific (as evidenced by the absence of H3K27ac in naive B [NB] cells and strong H3K27ac marks in GC cells; Figure 1F). Because CE1 showed the strongest occupancy of OCT2, OCA-B, and MEF2B (Figure 1F), it was selected for further analyses. ChIP-qPCR revealed decreased H3K27ac levels at CE1 after CRISPRi knockdown of either of the three factors (Figure 2H), whereas no difference was observed at a negative region (NR) 41 kb upstream of the *BCL6* promoter (Figure S6). Similarly, enhancer RNA (eRNA) expression (Core et al., 2014; Wang et al., 2011) from CE1 and other LCR constituent enhancers was decreased after CRISPRi knockdown of OCT2, OCA-B, or MEF2B (Figure S2B), suggesting that all three factors are required for full activation of *BCL6* LCR constituent enhancers. To test whether OCT2, OCA-B, and MEF2B can activate transcription through CE1, a derived 232-bp fragment centered on the OCA-B summit and containing 3 putative OCT2 sites (CE1\_O2-4; Figure S3B) was placed downstream of a luciferase reporter (Ighluc) driven by an octamer-containing *IgH* promoter (Figure 2I) and serves as a model for OCT2-regulated promoters, including *BCL6* (Stauss et al., 2016). Luciferase assays with this reporter (Ighluc-CE1\_O2-4) and with Ighluc were performed in OCT1-expressing HEK293T cells that do not express endogenous OCT2, OCA-B, or MEF2B (data not shown), and overexpression of these latter proteins was confirmed by immunoblot (Figure S2C).

The promoter-only reporter (Ighluc) was activated by expression of OCT2 and OCA-B (Figure 2J, lane 7 versus lane 1), as expected (Schubart et al., 1996), whereas further addition of MEF2B had only a very modest effect (Figure 2J, lane 10 versus lane 7). Importantly, although expression of OCA-B and OCT2 only modestly enhanced transcription on the CE1-containing Ighluc-CE1\_O2-4 template relative to the promoter-only Ighluc template (Figure 2J, lane 8 versus lane 7), addition of MEF2B yielded markedly greater induction (Figure 2J, lane 11 versus lane 10), indicating that optimal CE1 activity requires OCT2, OCA-B, and MEF2B. In further support, the MEF2B-mediated CE1 enhancer function depended on OCA-B (Figure 2J, lane 11 versus lane 23) and an intact O3 site (Figure 2J, lane 12 versus lane 11), indicating that MEF2B-mediated activation of CE1 re-

quires OCA-B and OCT2. These results indicate that OCT2, OCA-B, and MEF2B are critical for optimal *BCL6* LCR activity and consequent *BCL6* induction in an octamer element-dependent manner.

### OCT2, OCA-B, and MEF2B Bind Cooperatively to the *BCL6* LCR through Octamer Elements

The preceding results led us to hypothesize that recruitment of MEF2B to CE1 is either direct, through binding to a non-canonical MEF2B motif that requires functional cooperation with OCT2 or OCA-B, or indirect, through primary interactions with other TFs (e.g., OCT2). Consistent with the latter possibility, *de novo* motif analysis of publicly available MEF2B ChIP-seq datasets (Brescia et al., 2018; Ryan et al., 2015) revealed highly significant enrichment for motifs that closely match the canonical octamer binding motif for OCT1/2 (Figure S3A), suggesting that MEF2B might cooperate with OCT2 at regions enriched with octamer elements, at least in the GC B cell context. To define the CE1 elements important for OCT2 and MEF2B binding, recombinant FLAG-tagged OCT2 (F:OCT2) or MEF2B (F:MEF2B) proteins (Figures S3C and S3D) were incubated with immobilized biotin-conjugated CE1 DNAs bearing serial deletions of the four OCT2 binding motifs and two weak MEF2B motifs (Figure S3B). These immobilized template assays (ITAs) revealed that the strongest OCT2 motif (O3) is most critical for F:OCT2 binding (Figure 3A, top panel), whereas F:MEF2B showed apparent non-specific (OCT2 motif- and MEF2B motif-independent) binding (Figure 3A, bottom panel) at a low KCl concentration (150 mM). This binding was lost under more stringent ionic conditions (Figure 3B, lane 3 versus lane 7), consistent with the absence of strong MEF2B motifs on CE1 (Figure S3B).

Although we observed a high overlap of OCT2 and MEF2B binding peaks at CE1 (Figure 1F) as well as an OCT2 and OCA-B requirement for MEF2B-dependent CE1 enhancer activity (Figure 2J), we did not observe increased F:MEF2B binding to the CE1 fragment in the presence of F:OCT2 (Figure 3B, lanes 9–11 versus lanes 6–8), suggesting that the additional presence of OCA-B may be required. In a further analysis, mutation of the critical octamer motif O3 strongly reduced F:OCT2 binding (Figure 3C, lanes 5–8) but not the weak F:MEF2B binding (Figure 3C, lanes 3 and 4 and 7 and 8). These results suggest weak, non-specific binding of MEF2B alone in the assay and an OCA-B requirement (in addition to OCT2) for stronger, more specific binding. Indeed, consistent with the reporter assay results, F:MEF2B binding to CE1 was greatly enhanced by addition of recombinant FLAG-tagged OCA-B (F:OCA-B) (Figure S3E) in the presence of F:OCT2 (Figure 3C, lane 11 versus lane 7), and the whole complex was lost in the absence of the intact OCT2 motif (Figure 4F, lane 11). These results indicate a critical role of OCA-B in bridging MEF2B to OCT2 and OCT2 motif-dependent binding of MEF2B to CE1. Complementary GST pull-down assays

(C) Density metaplots of OCT2 or OCA-B ChIP-seq peaks at primed, active, and super enhancers.

(D) *De novo* motif analyses of OCT2 or OCA-B ChIP-seq peaks.

(E) Loading of OCT2 or OCA-B on enhancers in OCI-Ly7 cells.

(F) Genome browser view of the *BCL6* locus with tracks for various ChIP-seq in naive B (NB) cells, germinal center B cells (GCBs), or OCI-Ly7 cells. Constituent enhancers (CEs) are shaded in gray. Differential expression of TFs and cofactors from NB to GCB is color coded.

See also Figure S1.

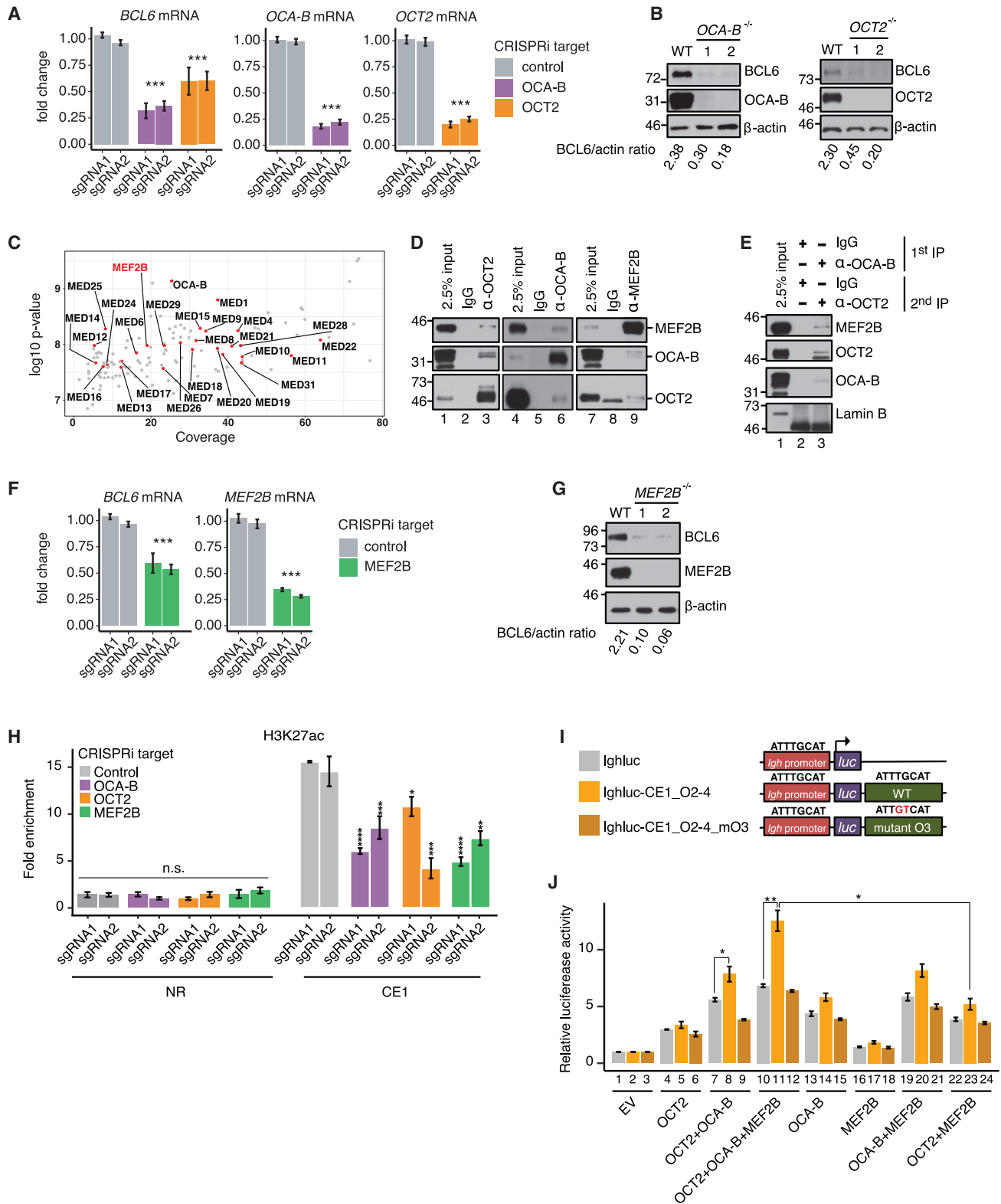


**Figure 2. OCA-B Binds to MEF2B to Drive BCL6 LCR Activity**

(A and F) *BCL6* mRNA levels quantified by qRT-PCR in CRISPRi knockdown of OCA-B (A), OCT-2 (A), and MEF2B (F) in OCI-Ly7 cells. Error bars represent mean  $\pm$  SD (n = 3).

(legend continued on next page)

with purified recombinant proteins (Figure S3F) showed not only direct, high-salt-sensitive binding of F:MEF2B to F:OCA-B (Figure 3D, lanes 8–10) but also increased binding in the presence of F:OCT2 under more stringent (200 mM KCl) conditions (Figure 3D, lane 12 versus lanes 9 and 6), indicating further levels of cooperative binding between these three proteins for stable complex formation.

To further investigate cooperative interactions of these factors, we performed electrophoretic mobility shift assays (EMSA) using the purified recombinant proteins and a 50-bp probe centered at M2/O3 from CE1 (CE1\_O3; Figure S3B). Consistent with the ITA results, OCT2, but not MEF2B, formed a stable complex with CE1\_O3 alone (Figure 3E, lanes 2 and 3). As expected, OCA-B did not bind CE1\_O3 alone but, in the presence of OCT2, induced a further shift indicative of a DNA·OCT2·OCA-B complex (Figure 3E, lanes 4 and 5). In contrast, MEF2B neither shifted the OCT2 band nor formed a DNA-bound complex with OCA-B (Figure 3E, lanes 6 and 7), even over a range of protein concentrations (Figure S3G). However, inclusion of MEF2B with OCT2 and OCA-B induced a probe shift indicative of a DNA·OCT2·OCA-B·MEF2B complex (Figure 3F, lanes 2–4). The octamer-dependent formation of this complex was confirmed by oligonucleotide competition with an unlabeled control probe (wild type [WT]), a mutant O3 probe (mt), and a non-specific probe adjacent to CE1\_O3 (ns) (Figures 3F, lanes 5–7, and S3H; see also legends for Figures 3F and S3H) and by an EMSA with a mutant O3 probe (CE1\_O3\_mut; Figure 3G, lane 9 vs. lane 4).

The above results indicate that MEF2B is recruited to DNA through OCT2 and OCA-B. However, it remained unclear whether the DNA binding ability of MEF2B is required for this recruitment and formation of the OCT2·OCA-B·MEF2B complex on DNA. To address this question, we purified a recombinant double mutant protein, MEF2B(D83V,Y69H), from insect cells (Figure S3I). The MEF2B D83V mutation has been shown previously to drastically reduce DNA binding at MEF2B sites, whereas the Y69H mutation had little effect (Pon et al., 2015). Consistent with the results of Pon et al. (2015), MEF2B(D83V,Y69H) showed no direct DNA binding ability (Figure S3J). The EMSA (Figure 3G) and ITA (Figure 4F) demonstrated that the mutant retains the ability to associate with the OCA-B·OCT2·octamer DNA complex, indicating that recruitment of MEF2B by OCA-B·OCT2 onto an octamer sequence is independent of its DNA binding property. We also observed that this mutant actually has a higher affinity for OCA-B (Figure S3K, lanes 8–10 versus lanes 3–5), consistent with formation of a more stable complex (Figure 3G, compare lane 5 with lane 4).

Although the MEF2B(D83V) mutant has impaired DNA binding ability (Figure S3J; Pon et al., 2015), the majority of the MEF2B-

occupied sites were retained in ChIP-seq experiments comparing MEF2B WT and MEF2B(D83V) (Brescia et al., 2018). We hypothesized that the retained MEF2B(D83V)-occupied sites are sites where MEF2B is recruited through other TFs and coactivators, such as OCT2 and OCA-B. To test this hypothesis, we first identified peaks bound by MEF2B without OCT2 or OCA-B ( $n = 4,128$ ) or by OCT2, OCA-B, and MEF2B together ( $n = 6,393$ ) and then calculated the fraction of peaks that are retained in the MEF2B D83V mutant. Sites bound by MEF2B, OCT2, and OCA-B together were approximately twice as likely to retain binding of the MEF2B(D83V) mutant ( $OR = 2.13$ ,  $p = 4.39e-79$ ; Figure S3L). In contrast, sites bound by MEF2B without OCT2 or OCA-B were far less likely to be retained in the MEF2B(D83V) mutant (odds ratio [OR] = 0.507,  $p = 4.94e-68$ ; Figure S3L). These results are consistent with our *in vitro* results and indicate that the DNA-binding ability of MEF2B is dispensable at sites where MEF2B is recruited through OCT2 and OCA-B.

To determine whether this OCA-B-dependent ternary CE1 complex occurs naturally in B cells, we performed ChIP-qPCR in *OCA-B*<sup>-/-</sup>, *OCT2*<sup>-/-</sup>, or *MEF2B*<sup>-/-</sup> OCI-Ly7 cells and measured fold enrichment at CE1 or NR. Consistent with our *in vitro* findings, full recruitment of MEF2B depended on OCT2 (Figure 3H) and OCA-B (Figure 3I). Notably, maximal OCT2 binding to CE1 was also impaired in the absence of MEF2B (Figure 3J) or OCA-B (Figure 3K). OCA-B recruitment was impaired not only by the absence of OCT2, as expected (Figure 3L), but also by loss of MEF2B (Figure 3M), suggesting that stable formation of the CE1 ternary complex requires all three components in the context of natural chromatin. To confirm this interdependency, we performed OCA-B ChIP-re-ChIP experiments in OCI-Ly7 cells using MEF2B or OCT2 antibodies for the first round of enrichment. In both cases, further IP with OCA-B antibodies enriched for CE1 binding (Figures 3N and S3M). Taken together, the results indicate that MEF2B forms a complex with OCT2 and OCA-B at octamer sites in an OCA-B-dependent manner.

### OCA-B Recruits the Mediator to *BCL6* LCR Constituent Enhancers

Although the preceding results established cooperative functions of OCT2, OCA-B, and MEF2B at the *BCL6* LCR, the mechanisms by which they activate target gene transcription from such a long distance (over 150 kb) remained unclear. Relevant to this issue, our IP-MS studies identified an association of OCA-B with a majority of the ~30 subunits of the Mediator complex (Figure 2C; Table S1), which has been implicated in enhancer-promoter communication (Malik and Roeder, 2016). To further explore the OCA-B-Mediator association, we

(B and G) *BCL6* protein levels measured by immunoblot following CRISPR knockout of OCA-B (B), OCT2 (B), and MEF2B (G) in OCI-Ly7 cells.

(C) OCA-B-associated proteins identified by IP-MS with an anti-OCA-B antibody in OCI-Ly7 cells. Significance was measured by comparison with signals from normal rabbit IgG antibody.

(D) Association of MEF2B with OCA-B or OCT2 in OCI-Ly7 nuclear extracts measured by reciprocal coIP with the indicated antibodies.

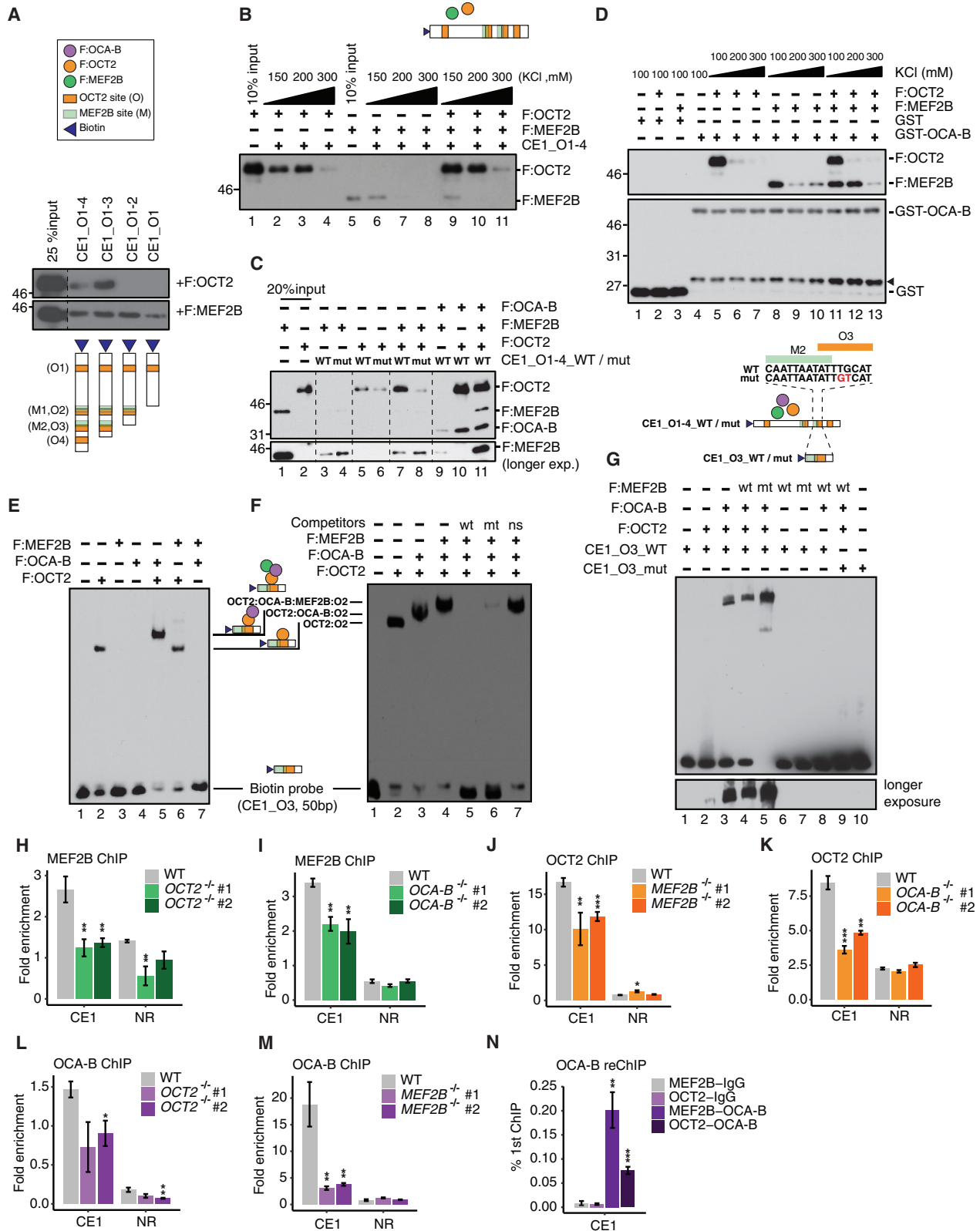
(E) Association of MEF2B with the OCT2+/OCA-B+ complex by double IP with the indicated antibodies.

(H) ChIP-qPCR for H3K27ac following CRISPRi knockdown of the indicated factors in OCI-Ly7 cells. Error bars represent mean  $\pm$  SD ( $n = 3$ ).

(I) Schematic of reporter constructs in (J).

(J) Luciferase reporter assays in 293T cells overexpressing the indicated factors. Error bars represent mean  $\pm$  SEM ( $n = 3$ ). Two-sided t test was used. p values are depicted with asterisks (\* $p < 0.05$ , \*\* $p < 0.01$ , and \*\*\* $p < 0.001$ ).

See also Figure S2.



(legend on next page)

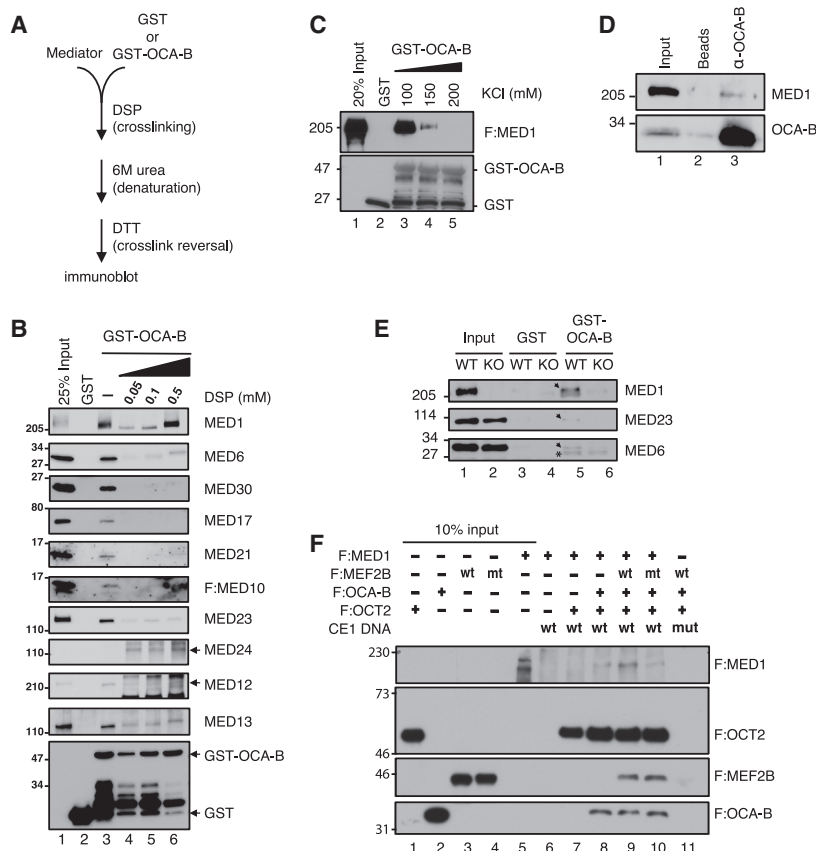


**Figure 4. OCA-B Recruits the Mediator to the *BCL6* LCR CE1**

(A) Schematic of the crosslinking-coupled binding assay. (B) Direct binding of OCA-B to the Mediator, measured by crosslinking-coupled binding assay using recombinant OCA-B and affinity-purified Mediator. (C) Direct binding of recombinant MED1 to OCA-B in the GST pull-down assay. (D) Association of MED1 with OCA-B in OCI-Ly7 nuclear extracts, measured by coIP using an anti-OCA-B antibody. (E) MED1-dependent binding of Mediator to recombinant OCA-B in nuclear extract from WT versus *Med1*<sup>-/-</sup> (knockout [KO]) mouse embryonic fibroblasts. (F) MEF2B-facilitated, octamer-dependent, and OCA-B-dependent binding of MED1 to octamer-bound OCT2 on CE1\_O2-4, measured by ITA. See also Figure S4.

performed reversible crosslinking-coupled binding assays (Figure 4A; detailed in STAR Methods; Kim et al., 2006) using recombinant glutathione S-transferase (GST)-OCA-B and a purified Mediator complex (Figure S4A). Multiple Mediator subunits indicative of complete Mediator bound to GST-OCA-B in the absence of the crosslinking procedure (Figure 4B, lane 3), whereas the crosslinking analysis with dithiobis(succinimidyl propionate) (DSP) indicates that MED1 interacts directly with OCA-B (Figure 4B, lanes 4–6). This direct interaction was further confirmed by a GST pull-down assay with purified GST-OCA-B and FLAG-tagged MED1 (F:MED1) (Figures 4C and S4B). CoIP

further showed an association of endogenous OCA-B with MED1/Mediator in OCI-Ly7 nuclear extracts (Figure 4D). In contrast, Mediator subunits could not be pulled down by OCA-B in nuclear extract from murine *Med1*<sup>-/-</sup> embryonic fibroblasts (Figure 4E; Ito et al., 2000), confirming that MED1 is the primary interacting subunit of Mediator for OCA-B. ITAs using the CE1\_O2-4 probe and recombinant proteins also demonstrated an OCA-B requirement for MED1 recruitment by OCT2 (Figure 4F, lane 8 versus lane 7), and addition of MEF2B

### The *BCL6* LCR Must Be Positioned in *cis* to Allow GC Formation *In Vivo*

Because of the large genomic distance (>150 kb) between the *BCL6* promoter and the *BCL6* LCR, we asked whether LCR function was limited to the same allele (i.e., acting in *cis*) or could

**Figure 3. OCT2, OCA-B, and MEF2B Bind Cooperatively to the *BCL6* LCR through Octamer Elements**

(A and B) Binding of OCT2 or MEF2B at 150 mM KCl (A) or both at 150, 200, and 300 mM KCl (B) on CE1 DNA with serially deleted fragments (Figure S3B), measured by ITA. (C) Cooperative binding of OCT2, OCA-B, and MEF2B to CE1\_O1-4 DNAs with wild-type (WT) or O3 octamer-mutated (mut) DNAs, measured by ITA. (D) MEF2B and/or OCT2 binding to OCA-B, measured by GST pull-down assay. An arrowhead indicates the degradation product of GST-OCA-B. (E–G) Measurement of stable (octamer-dependent) protein-DNA complexes by EMSA with a 50-bp DNA probe, CE1\_O3. Non-biotinylated DNA probes from WT O3, mut O3, or an adjacent sequence of O3 (ns) were used as cold competitors in (F), and an O3 octamer-mut probe (CE1\_O3\_mut) was included in (G). The OCT2-CE1\_O3 complex is visible on a longer exposed film at the bottom of (G). The anomalous competition by the mut octamer probe in (F), lane 6, reflects use of an excessive (100x) amount of competitor, with octamer dependency revealed more clearly in (G) and in Figure S3H with mutant octamer probes and/or lower amounts (2–5x) of competitor, respectively. (H–M) Occupancy of MEF2B, OCT2, and OCA-B on CE1, measured by ChIP-qPCR analysis of MEF2B (H and I), OCT-2 (J and K), and OCA-B (L and M) binding to CE1 in WT cells and *OCT2*<sup>-/-</sup> (H and L), *OCA-B*<sup>-/-</sup> (I and K), or *MEF2B*<sup>-/-</sup> (J and M) in OCI-Ly7 cells. NR, negative control region 41 kb upstream of the *BCL6* transcriptional start site (TSS). (N) OCA-B and MEF2B co-occupancy, measured by ChIP-re-ChIP-qPCR, using anti-MEF2B or anti-OCT2 as the first antibody and anti-OCA-B antibody as the second antibody. (H–N) Error bars represent mean ± SEM (n = 3). Two-sided t test was used. p values are depicted with asterisks (\*p < 0.05, \*\*p < 0.01, and \*\*\*p < 0.001). See also Figure S3.

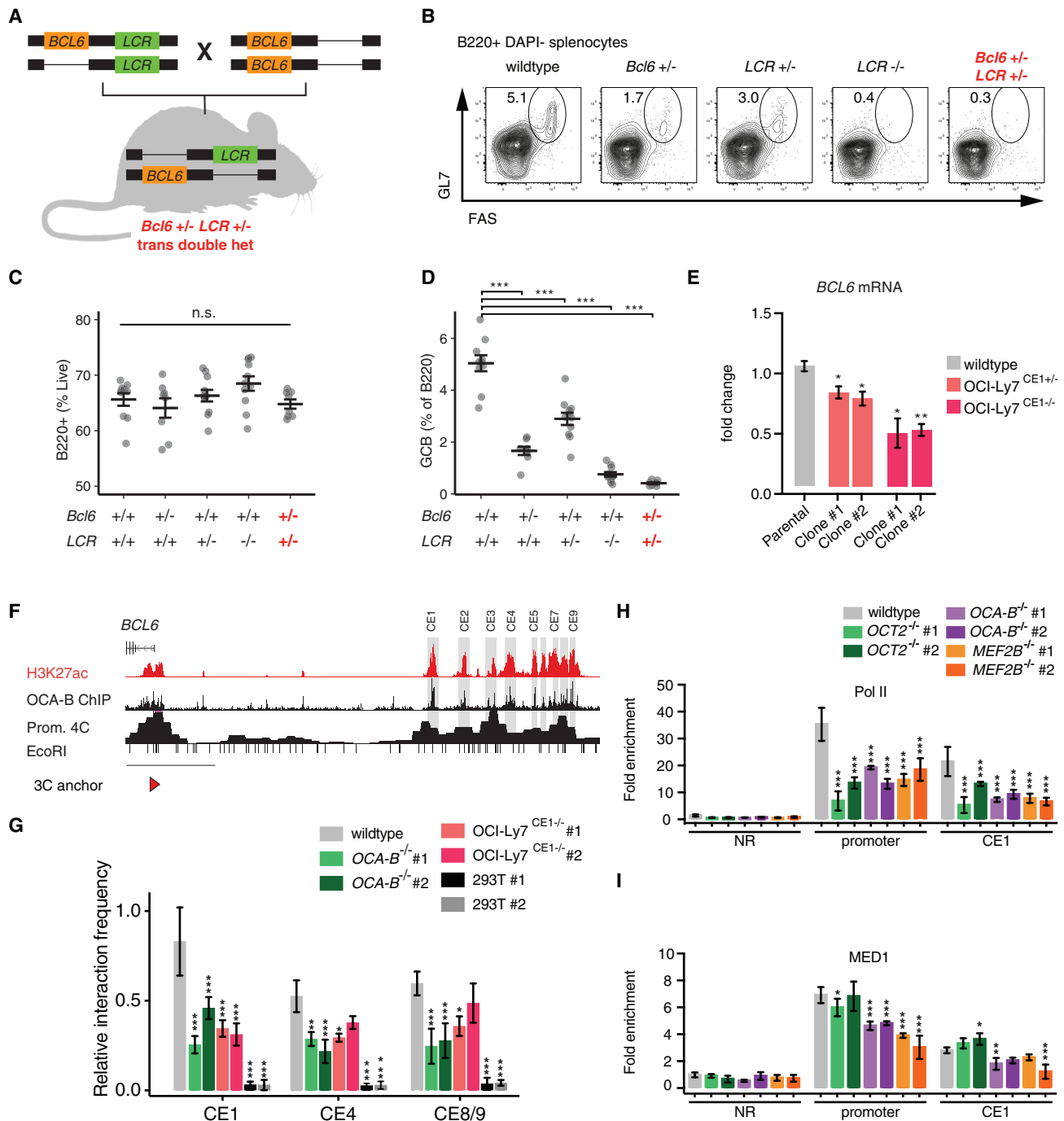


**Figure 5. The *Bcl6* LCR Must Be Positioned in *cis* to Allow GC Formation In Vivo**

(A) Mating strategy used to obtain *Bcl6* KO combined with *Bcl6*-LCR KO on separate alleles (i.e., in *trans*). (B–D) GC formation after sheep red blood cell (SRBC) immunization in WT, *Bcl6*<sup>+/-</sup>, *LCR*<sup>+/-</sup>, *LCR*<sup>-/-</sup> and trans double heterozygous mice (the latter is highlighted in red) as shown by representative flow cytometry plots (B) and quantification of B220<sup>+</sup> splenocytes (C) and GL7<sup>+</sup>FAS<sup>+</sup> splenic GCBs (D). (E) Relative *BCL6* mRNA levels in WT, *CE1*<sup>+/-</sup>, or *CE1*<sup>-/-</sup> OCI-Ly7 cells. (F) Genome browser view of the *BCL6* locus with tracks for H3K27ac and OCA-B ChIP-seq in OCI-Ly7 cells and circular chromosome conformation capture sequencing (4C-seq) anchored on the *BCL6* promoter in GCBs. (G) Contact frequency between the *BCL6* promoter (anchor) and the indicated LCR CEs, measured by 3C-qPCR in WT, *CE1*<sup>-/-</sup>, or OCA-B $^{-/-}$  OCI-Ly7 cells. HEK293T cells were used as a negative control.

(legend continued on next page)

exert control over the sister chromosome (i.e., acting in *trans*). To test this, we crossed  $LCR^{-/-}$  mice with  $Bcl6^{-/-}$  mice to produce “compound”  $Bcl6^{-/+};LCR^{+/-}$  heterozygous animals with  $Bcl6$  knockout on one allele and LCR knockout on the other allele (i.e., *trans* configuration; Figure 5A).  $Bcl6^{-/-}$  and  $LCR^{-/-}$  mice manifest complete loss of GCs (Bunting et al., 2016; Dent et al., 1997; Fukuda et al., 1997; Ye et al., 1997). In these compound heterozygous mice, if the  $Bcl6$  LCR were able to interact in *trans*, then the WT LCR located on the  $Bcl6^{-}$  chromosome would rescue expression of  $Bcl6$  on the  $LCR^{-}$  DNA strand. To test whether this could occur, we compared and contrasted GC formation in mice with the following genotypes:  $Bcl6^{-/+};LCR^{+/-}$ ,  $Bcl6^{-/+}$  and  $LCR^{+/-}$ . We also included  $Bcl6^{+/+};-LCR^{+/+}$  and homozygous  $LCR^{-/-}$  mice as negative and positive controls, respectively. Groups of mice with the respective genotypes were immunized with T cell-dependent antigen (sheep red blood cells) to induce GC formation and sacrificed 10 days later, when GC reaction is at its peak. Splens from these mice were then examined by flow cytometry to assess the abundance of GC B cells (Figure 5B). As expected, the total numbers of B cells ( $B220^{+}$ ) were equivalent in these mice (Figure 5C). As reported previously,  $Bcl6^{+/+}$  mice display a partial reduction in the abundance of GC B cells ( $B220^{+}, Fas^{+}, GL7^{+}$ ) (Huang et al., 2014). Similarly,  $LCR^{+/-}$  mice show a partial reduction in GC B cells (Figure 5D). Compound (*trans*) heterozygous  $Bcl6^{-/+};LCR^{+/-}$  mice, however, manifest complete abrogation of the GC reaction (Figure 5D), similar to the GC defect observed in  $LCR^{-/-}$  mice. Thus,  $Bcl6$  and its neighboring LCR must be located on the same chromosome to function *in vivo*, supporting a direct, *cis*-regulatory role of the LCR in induction of  $Bcl6$  and GC formation.

### **BCL6 LCR Architectural Functions Require OCA-B and Ternary Complex-Bound Enhancer Elements**

In GC B cells, the  $BCL6$  LCR makes extensive contacts with the  $BCL6$  promoter and other GC-associated genes located along chromosome 3 (Bunting et al., 2016). This prominent architectural function, together with the direct, *cis*-regulatory role of the  $BCL6$  LCR observed above, prompted us to investigate whether *cis*-regulatory elements within the LCR, such as CE1, are essential for LCR architectural effects. To test this, we first established CE1-depleted OCI-Ly7 cells (OCI-Ly7<sup>CE1+/-</sup> and OCI-Ly7<sup>CE1-/-</sup>) by CRISPR and observed reduction of  $BCL6$  expression (Figure 5E). Architectural effects were calculated by measuring the interaction frequency between the  $BCL6$  promoter as an anchor and different regions across the LCR using chromosome conformation capture (3C) as described (Ramachandrarreddy et al., 2010; Figure S4C). For all tested constituent enhancers with high interactivity (Figures 5F and S4D), OCI-Ly7<sup>CE1+/-</sup> cells lost significant promoter interactivity with the region around CE1 (Figure 5G), whereas no interactivity was shown in control HEK293T cells because of the inactive state of the H3K27ac-negative LCR (The Encyclopedia of DNA Elements; data not shown). Because OCA-B is critical for  $BCL6$  expression (Figures

2A and 2B) and LCR activity (Figure 2J), we hypothesized that loss of OCA-B would affect  $BCL6$  enhancer-promoter contacts. In confirmation, CRISPR-mediated or short hairpin RNA (shRNA)-mediated depletion of OCA-B also significantly reduced enhancer-promoter contacts for all tested constituent enhancers (Figures 5G and S4D, respectively).

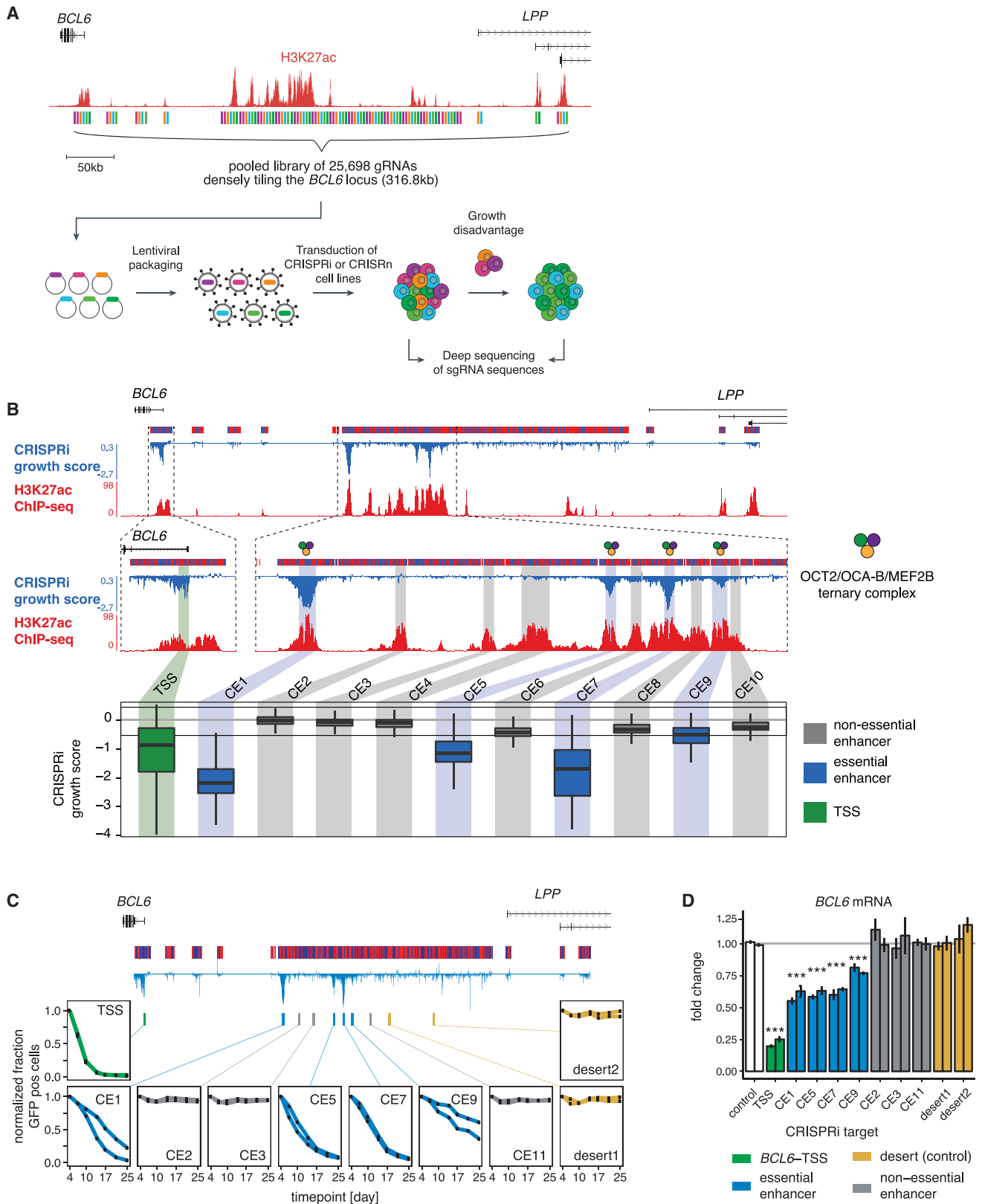
The Mediator is thought to function as a signal transducer that facilitates flow of regulatory information from enhancers to promoters (Malik and Roeder, 2016). Although MED1 has been reported to be essential for certain enhancer-promoter contacts (Lai et al., 2013), recent provocative studies based on degron-mediated rapid disassembly of Mediator have argued for a functional role by a still unclear mechanism rather than a stable architectural bridging role in enhancer-dependent regulation of promoter activity (El Khattabi et al., 2019; Jaeger et al., 2020). Nevertheless, transient knockdown of OCA-B (Figure S4F) also led to a striking loss of Mediator at OCA-B peaks across the LCR (Figure S4E), suggesting that OCA-B is required for Mediator recruitment and  $BCL6$  enhancer-promoter interactivity, both of which are crucial for  $BCL6$  activation. The key downstream event related to Mediator recruitment and enhancer-promoter communication is formation of a stable RNA polymerase II (RNA Pol II) pre-initiation complex that leads to induction of target gene transcription. Accordingly, significant decreases in RNA Pol II and MED1 occupancy at the  $BCL6$  promoter were observed in most of the CRISPR clones, with the exception of persistent MED1 occupancy in  $OCT2^{-/-}$  OCI-Ly7 cells (Figures 5H and 5I) that likely reflects potential compensation by OCT1. These results suggest a critical role of OCA-B and CE1 in supporting the  $BCL6$  LCR architectural function and facilitating formation of transcriptional complexes at the promoter through recruitment of the Mediator, whether by means of transient bridging action or through engendering formation of activator-coactivator condensates in the vicinity of the promoter (Shrinivas et al., 2019).

### **CRISPRi Screening of the BCL6 LCR Reveals Internal Hierarchy and Essential Enhancer Elements Highly Enriched with the Ternary OCT2·OCA-B·MEF2B Complex**

The critical role of CE1 and the ternary complex on LCR activity prompted us to further study the role of other LCR constituent enhancers and their relationship to the ternary complex. To this end, we performed dCas9-KRAB-mediated CRISPRi screens, leveraging the fact that  $BCL6$  is essential for cell survival and proliferation in GC B cells and GC-derived lymphoma cell lines such as OCI-Ly7 (Figure 6A). We generated a pooled gRNA library, densely tiling all potential regulatory elements at the human  $BCL6$  locus, covering a genomic region of 316.8 kb with 25,698 gRNAs in total (Figure 6A). The efficacy of the screen was validated by gRNAs targeting 100 essential genes (Figure S5A). Correlation between replicates was high, indicating robust and reproducible screening results

(H and I) Occupancy of RNA Pol II (RPB1, H) or Mediator (MED1, I) on the  $BCL6$  promoter and CE1 region, measured by ChIP-qPCR using the indicated antibodies in WT versus  $OCA-B^{-/-}$ ,  $OCT2^{-/-}$ , or  $MEF2B^{-/-}$  OCI-Ly7 cells.

Error bars represent mean  $\pm$  SEM (n = 3). Two-sided t test was used. p values are depicted with asterisks (\*p < 0.05, \*\*p < 0.01, and \*\*\*p < 0.001). See also Figure S4.



(legend on next page)

(Pearson correlation  $r = 0.81$ ; [Figure S5B](#)). Notably, disruptions of a majority of the constituent enhancers showed no growth defects, indicating that they are non-essential enhancers (NEs) for cell growth or survival. However, four constituent enhancers, including CE1, had mean growth scores lower than the first percentile of control gRNA growth scores and, thus, were classified as essential enhancers (EEs) ([Figure 6B](#)). Consistent with the results of the screen, independent validations revealed no dropouts for any of the NE enhancers ([Figure 6C](#)), and these results were confirmed in another GC B cell (GCB)-DLBCL cell line (SU-DHL-4) ([Figure S5C](#)). Because NEs could potentially produce effects too small to pick up as a growth phenotype, we wanted to find out whether simultaneous perturbation of two NEs would produce measurable growth defects. To this end, we transduced cells with two separately labeled gRNAs and assessed growth over time. Notably, no growth defect was observed whenever the CE2 NE and another NE were disrupted jointly, whereas growth defects were maintained when an EE was disrupted jointly with CE2 ([Figure S5D](#)). Importantly, only disruption of EEs had a significant effect on *BCL6* mRNA levels, whereas NEs were dispensable ([Figure 6D](#)). These results indicate a strong internal hierarchy and demonstrate that the *BCL6* LCR activity relies completely on distinct EE elements.

The aforementioned results raise the question of how EEs differ from NEs. To address this, we compared several features related to functions of a regulatory element. Although monomethylation of histone H3 at lysine 4 (H3K4me1), trimethylation of histone H3 at lysine 4 (H3K4me3), and MED1 levels are indistinguishable between NEs and EEs, we observed higher (but not statistically significant) intensities of H3K27ac marks, DNA accessibility measured by DNase I hypersensitive site sequencing (DNase-seq), and eRNA signals for EEs relative to NEs ([Figures S5E and S6](#)). On the other hand, MEF2B showed a striking enrichment at EEs, whereas OCT2 and OCA-B showed higher but not statistically significant occupancy at EEs versus NEs ([Figures S5F and S6](#)). Together with our detailed characterization of the OCT2·OCA-B·MEF2B complex described above, this indicates that a key distinguishing feature of EEs is high enrichment of the OCT2·OCA-B·MEF2B complex. Supporting the above observations, a significantly higher density of octamer motifs was measured in EEs compared with NEs ([Figure S5G](#)), providing additional evidence of the use of octamer motifs in establishing LCR activity. Together, these data indicate that octamer motif density and binding of the OCT2·OCA-B·MEF2B ternary complex are key distinguishing factors of *BCL6* LCR EEs critical for their function.

## DISCUSSION

In relation to the profound importance of GCs for humoral immunity and lymphoma pathogenesis, our major objective has been to understand gene-regulatory pathways important for GC formation. In the present study, analyses of gene targets and mechanisms for the GC-specific master regulator OCA-B converged with analyses of the GC-specific LCR on the gene encoding the master regulator *BCL6*. Genomic analyses of OCA-B and its GC-enriched DNA-binding partner OCT2 showed predominant binding to superenhancers, including the *BCL6* LCR, in GC-derived DLBCL cells and also established colocalization with the GC-selective TF MEF2B. Complementary biochemical and genetic analyses further identified an OCA-B·OCT2·MEF2B ternary complex that proved to be essential for optimal activation of the *BCL6* LCR through OCT2-binding (octamer) elements. Mechanistically, this complex was shown to function through OCA-B-MED1/Mediator interactions, leading to *BCL6* LCR-promoter communication. In parallel studies focused on the structure and function of the large LCR, a densely tiled CRISPRi screen established that only a specific subset of the LCR constituent enhancers is important for proliferation and survival of DLBCL cells and for *BCL6* expression, and the critical subset of enhancers was characterized by high ternary complex occupancy and a high density of octamer motifs. Based on these results, we report a previously unidentified GC-specific transcription complex and essential elements controlling the activity of a GC-specific LCR of a critical GC master regulator. Further details and implications of these findings are discussed below.

### Control of Optimal *BCL6* Expression by the OCT2·OCA-B·MEF2B Ternary Complex

All three components of this ternary complex are essential in numerous DLBCL cell lines (DepMap release 20Q2; data not shown). In fact, the top two co-dependencies of OCT2 are MEF2B and OCA-B, confirming their intimate functional relationship. This strong dependency of DLBCL cell lines on the ternary complex components might arise from their own independent functionalities or, at least in part and as suggested here, from their cooperative roles in *BCL6* activation. Although optimal *BCL6* LCR-directed *BCL6* expression during GCB differentiation has been thought to involve GC-specific factors, so far they have not been well defined. Several previous studies have examined the role of *Pou2af1* in *Bcl6* expression in mouse B cells, but none involved analyses in cells with characteristics of GCBs ([Qin et al., 1998](#); [Corcoran et al., 2005](#); [Hodson et al., 2016](#); [Levels et al., 2019](#)). A recent study has linked OCT2 and OCA-B to *Bcl6* promoter activity in mouse follicular T helper cells, whose

### Figure 6. Functional Dissection of the *BCL6* LCR Reveals Essential Enhancer Elements Bound by the Ternary Complex

(A) Schematic representing the screening strategy and overview of the screened region and H3K27ac ChIP-seq signal as a surrogate for regulatory elements. (B) Genome browser view of CRISPRi screening results along with H3K27ac ChIP (top). *BCL6* LCR CEs are categorized as EEs when the mean growth score is lower than the first percentile of control gRNA growth scores (1<sup>st</sup>–99<sup>th</sup> percentile indicated by horizontal lines, bottom panel). TSS, *BCL6* transcriptional start site. (C) Effect of CRISPRi-mediated perturbation of individual CEs, the TSS, and two negative control regions (deserts) on cell growth. gRNA-expressing cells are GFP positive, and the fraction of GFP positive cells was monitored by flow cytometry over time. (D) Effect of CRISPRi-mediated perturbation of individual CEs, the TSS, and deserts on *BCL6* expression, as determined by qPCR. Error bars represent minimal/maximal values of biological replicates ( $n = 2$ ). Each region was targeted with two different gRNAs (C and D). Two-sided t test was used. p values are depicted with asterisks (\* $p < 0.05$ , \*\* $p < 0.01$ , and \*\*\* $p < 0.001$ ). See also [Figures S5 and S6](#).

differentiation and function also requires *Bcl6* (Stauss et al., 2016). However, *Bcl6* expression is much lower in these cells than in GCBs (Sayin et al., 2018), likely because of the lack of LCR activity (Weinstein et al., 2014). Here biochemical assays established physical interactions between OCT2, OCA-B, and MEF2B that manifest as formation of a ternary complex on OCT2 binding sites (octamer elements) in the *BCL6* LCR. Importantly, a corresponding co-occupancy of these factors on constituent *BCL6* LCR enhancers and functional cooperativity in *BCL6* expression have been demonstrated in DLBCL cells. It is noteworthy that the key DNA-binding elements for formation of this complex are the OCT2 binding sites, with no requirement for MEF2B sites and with MEF2B being recruited through direct interactions with OCT2-bound OCA-B and no apparent interactions with OCT2. Thus, the order of assembly of these key factors on DNA is OCT2→OCA-B→MEF2B.

The sequential function of these factors may be especially important during early differentiation of GCBs, where *BCL6* is repressed during early initiation and activated later as cells migrate and form nascent GCs (Calado et al., 2012; Dominguez-Sola et al., 2012). A hierarchical model of *BCL6* regulation through stepwise activation of the LCR can thus be proposed. First, specific constituent enhancers in the LCR are premarked with the lymphoid lineage OCT2, potentially acting as a pioneer factor or lineage-determining TF (data not shown). Upon antigen engagement and entry into the early GC initiation stage, induced OCA-B pre-activates the *BCL6* LCR, followed by full activation by MEF2B, which appears slightly later than OCA-B during GC initiation (De Silva and Klein, 2015).

### MEF2B as a Transcriptional Coactivator of the GC-Specific *BCL6* LCR

Given reports of MEF2B recruitment and function through MEF2 DNA binding motifs in GC transcription events (Ying et al., 2013; Brescia et al., 2018), it was surprising to find that MEF2B function is apparently independent of the MEF2 motif in the present study, at least on the *BCL6* LCR constituent enhancers. However, the lack of direct binding of MEF2B to CE1 and the dependence on OCT2 and OCA-B are consistent with a previous study showing GATA factor-MEF2 synergy independent of the DNA binding domain of MEF2 (Morin et al., 2000) as well as our demonstration that MEF2B can be recruited by a direct OCA-B interaction. Compared with other MEF2 family members, MEF2B differs by the presence of a glutamine in place of an aspartic acid at position 14, which affects a key DNA binding residue within the MADS box (Molkentin et al., 1996). This difference implies that MEF2B might have reduced DNA affinity (Pon and Marra, 2016), which may provide a higher capability for MEF2B genomic redistribution. Notably, MEF2B is recurrently mutated in GC-derived FLs and DLBCLs (Pastore et al., 2015; Ying et al., 2013). In this regard, the overwhelming majority of mutations affect the N-terminal DNA binding MADS and MEF2 domains, and the most common mutations, K4E and D83V, have been shown to decrease MEF2B binding to DNA (Pon et al., 2015). Although the MEF2 DNA binding domain has been shown to mediate physical and functional interactions with GATA factors (Morin et al., 2000), we found that the DNA binding-defective MEF2B(Y69H,D83V) not only retained but actually showed an

enhanced ability to interact with OCA-B and subsequent OCT2-bound OCT2 sites. This result suggests an alternative mechanism of pathogenesis for this recurrent mutation and mandates future studies to elucidate the OCA-B-MEF2B interface, which could potentially be targeted for therapeutic purposes.

Interestingly, the reduced OCA-B occupancy on CE1 in *MEF2B*<sup>-/-</sup> cells was not observed in the biochemical analysis, where MEF2B is dispensable for OCA-B binding to OCT2, implying an additional layer of regulation in cells. The possibility that MEF2B might regulate OCA-B expression is unlikely because a reduction of OCA-B is not observed in CRISPRi-mediated MEF2B knockdown cells. Therefore, a more likely possibility is that the intracellular chromatin structure of the LCR adds constraints to OCA-B-OCT2 interactions that are overcome by cooperative MEF2B interactions.

### OCA-B Recruitment of the Mediator as a Driver of LCR Functionality

Beyond identification of key transcription (co)factors involved in activation of *BCL6* through the LCR, a key question is how these factors stimulate transcription from the downstream promoter. Of major significance in this regard is our demonstration of physical and functional interactions of OCA-B with the MED1 subunit of the Mediator. Mediator serves as the major means of communication between enhancer-bound TFs and the general transcription machinery at the core promoter, establishing a functional pre-initiation complex (Allen and Taatjes, 2015; Levine et al., 2014; Malik and Roeder, 2016). Consistent with this view, our studies have shown (1) colocalization of MED1 with OCT2, OCA-B, and MEF2B on LCR constituent enhancers and (2) concomitant loss of LCR-promoter interactions, Mediator and RNA Pol II recruitment, and *BCL6* expression following loss of OCA-B. Although not eliminating potential interactions of other Mediator subunits with OCA-B or other components of the ternary complex, these results establish a clear role of MED1 in LCR-mediated *BCL6* expression.

MED1 has been shown to be essential for erythroid development, although no obvious effect on the lymphoid lineage was observed in *Mx-Cre/Med1*<sup>fl/fl</sup> mice (Stumpf et al., 2010). However, *ex vivo* culture of splenocytes treated with interleukin-4 and lipopolysaccharides from *Mb1-Cre/Med1*<sup>fl/fl</sup> mice showed a 30%–60% reduction in class-switch recombination (Thomas-Claudian et al., 2016), likely because of impaired interactions between the *E $\mu$*  enhancer and the  $\gamma$ 1 promoter (*IgG1*). In view of our previous observation that OCA-B can regulate transcription of class-switched *Ig* genes by acting on their promoters and enhancers, our current finding that OCA-B recruits Mediator via MED1 raises the possibility OCA-B may act in transcription or transcription-coupled class switch recombination at the *IgH* locus by a mechanism similar to that observed for the *BCL6* locus.

### Organizational Hierarchy of the Complex *BCL6* LCR Revealed by CRISPRi Screening

The enormous size of the *BCL6* LCR raises questions regarding the basis of the complexity, the possible necessity of all constituent enhancers for optimal *BCL6* expression, and potential redundancy for biological robustness. Our CRISPRi screening approach proved to be highly informative in

dissecting this complex non-coding locus. Use of a maximum-density gRNA library combined with CRISPRi provided a precise, robust, and quantitative assessment of the functional effect of each enhancer element within the *BCL6* LCR. We identified four distinct constituent enhancers that are essential for LCR activity and GCB-DLBCL survival (termed EEs), whereas all other constituent enhancers were absolutely dispensable or non-essential (termed NEs), revealing a striking hierarchy among the constituent enhancer elements. Depicting the characteristics of EEs showed no correlation with H3K4me1, H3K4me3, MED1 occupancy, and promoter interactivity and weak correlation with DNA accessibility, eRNA expression, and H3K27ac levels. These observations highlight the fact that general features of enhancer activity do not correlate with essential constituent enhancers in an LCR, at least in certain tissues, and suggest that the context of each element may be different as a result of variation in associated factors so that the magnitude of the activity of each element cannot be judged accurately by comparing the general features. Importantly, however, individual EEs showed strong OCT2, OCA-B, and MEF2B occupancy, potentially in the form of the identified ternary complex. Nonetheless, there likely exist additional factors that contribute to the function of EEs and may help distinguish them from NEs. Future studies will be required to elucidate the full complement of factors that drive and distinguish EEs in different LCRs and in different cell types.

Exactly how the ternary complex forms specifically at EEs remains unclear, but formation was linked significantly to high-density octamer motifs. It is notable that TF binding site (TFBS) density has been implicated recently as a driver of transcriptional condensate formation at enhancers (Shrinivas et al., 2019), a process that has been suggested to be of particular importance for super enhancer functions (Boija et al., 2018; Hnisz et al., 2017; Sabari et al., 2018) involving RNA Pol II, Mediator, and specific types of TFs. In agreement with this model, disruption of just one OCT2 site had a drastic effect on the transcriptional activity of CE1. Moreover, OCT2 and MEF2B consist largely of intrinsically disordered regions that, in other studies, have an established role in condensate formation. In light of these observations, one can speculate that *BCL6* LCR EEs, by virtue of their TFBS density, act as scaffolds that nucleate formation of transcriptional condensates containing OCT2, OCA-B, and MEF2B, with subsequent participation of Mediator and RNA Pol II. A possible role of MEF2B in condensate formation is further supported by the observation (Brescia et al., 2018) that all super enhancers in human GCBs are bound by MEF2B.

In summary, we uncovered a previously unknown cooperativity between OCT2, OCA-B, and MEF2B and identified the crucial functional units of the *BCL6* LCR, which are specifically enriched with an OCT2·OCA-B·MEF2B complex. Our results highlight how an intricate interplay of lineage- and stage-specific factors converges on specific and highly essential enhancer elements to drive the function of a cell-type-defining LCR.

## STAR★METHODS

Detailed methods are provided in the online version of this paper and include the following:

- **KEY RESOURCES TABLE**
- **RESOURCE AVAILABILITY**
  - Lead Contact
  - Materials Availability
  - Data and Code Availability
- **EXPERIMENTAL MODEL AND SUBJECT DETAILS**
  - Cell Lines
  - Mouse Models and Strains
- **METHOD DETAILS**
  - Crosslinked Chromatin Immunoprecipitation (ChIP) and ChIP-sequencing
  - Data analysis for ChIP-seq
  - Lentivirus Production, Transduction, and shRNA-Mediated Gene Knock-down
  - CRISPR/Cas9-mediated Gene Editing
  - Generation of CRISPRi Cell Lines
  - CRISPRi-mediated interference
  - RNA Isolation, cDNA preparation, and Quantitative real-time PCR (qPCR)
  - Luciferase Assay
  - Immunoprecipitation and Immunoprecipitation Mass Spectrometry (IP-MS)
  - Purification of Recombinant Proteins
  - Purification of the Mediator Complex from HeLa
  - Protein-protein Interactions and Reversible Crosslinking-coupled Binding Assays
  - Immobilized Template Assay
  - Electrophoresis Mobility Shift Assay (EMSA)
  - Immunization and FACS Analysis of GC B Cells
  - Chromosome Conformation Capture Assay (3C)
  - gRNA Library Design
  - gRNA Library Cloning
  - CRISPRi Screening
  - CRISPRi Screen Analysis
  - CRISPRi Screen Validation Experiments
  - Constituent-enhancer-based Analysis
  - Sequencing and Analysis of Chromatin-bound RNA (ChromRNA-seq)
  - Transcription Factor Binding Motif Analysis
- **QUANTIFICATION AND STATISTICAL ANALYSIS**

## SUPPLEMENTAL INFORMATION

Supplemental Information can be found online at <https://doi.org/10.1016/j.molcel.2020.10.036>.

## ACKNOWLEDGMENTS

C.-S.C. was supported by the Postdoctoral Research Abroad Program from the Ministry of Science and Technology, Taiwan. J.C.H. was supported by a Mildred Scheel postdoctoral fellowship from the German Cancer Aid, Germany and a postdoctoral fellowship from the National Cancer Center, United States. H.-Y.Y. was supported by a 2016 AACR-Takeda Oncology Fellowship in Lymphoma Research (16-40-38-YING) and the Postdoctoral Research Abroad Program from the Ministry of Science and Technology, Taiwan. A.M.M. was supported by NCI R35 CA220499, NCI P01 CA229086, LLS SCOR 7021-20, The Chemotherapy Foundation, The Samuel Waxman Cancer Research Foundation, and the Follicular Lymphoma Consortium. O.E. was supported by LLS SCOR 7021-20. R.G.R. was supported by NIH R01 CA163086, NIH R01 CA178765, NIH R01 AI148387, and LLS SCOR 7021-

20. This study makes use of data generated by the Blueprint Consortium. Blueprint funding was provided by the European Union Seventh Framework Program (FP7/2007–2013) under grant agreement 282510 BLUEPRINT. We would like to thank Neville Sanjana of the NYGC and NYU for crucial discussions and advice regarding CRISPR screening strategies. CRISPR guide library cloning was performed by the Gene Editing and Screening Core Facility at Memorial Sloan Kettering Cancer Center (New York, NY), which is supported by Cancer Center Support Grant P30 CA008748 S5. We thank Sohail Malik for critical discussions.

#### AUTHOR CONTRIBUTIONS

C.-S.C. and J.C.H. conceived and conducted most of the experiments, analyzed and interpreted data, and wrote the manuscript. R.S. conceived and performed animal experiments. H.-Y.Y. performed CRISPR knockout experiments. L.S. performed distance analysis of OCT2 motifs. M.R.T. analyzed the public MEF2B-D83V ChIP-seq data. A.M.M. and R.G.R. supervised the project and wrote the manuscript. All authors read the manuscript.

#### DECLARATION OF INTERESTS

A.M.M. receives research funding from Janssen and Sanofi Aventis, consults for Epizyme and Constellation, and is on the advisory board of KDAC Therapeutics. R.G.R. is a member of the Molecular Cell Advisory Board.

Received: April 15, 2020

Revised: September 9, 2020

Accepted: October 27, 2020

Published: November 23, 2020

#### REFERENCES

Allen, B.L., and Taatjes, D.J. (2015). The Mediator complex: a central integrator of transcription. *Nat. Rev. Mol. Cell Biol.* **16**, 155–166.

Bartholdy, B., Du Roure, C., Bordon, A., Emslie, D., Corcoran, L.M., and Matthias, P. (2006). The Ets factor Spi-B is a direct critical target of the coactivator OBF-1. *Proc. Natl. Acad. Sci. USA* **103**, 11665–11670.

Basso, K., and Dalla-Favera, R. (2015). Germinal centres and B cell lymphomagenesis. *Nat. Rev. Immunol.* **15**, 172–184.

Bhatt, D.M., Pandya-Jones, A., Tong, A.-J., Barozzi, I., Lissner, M.M., Natoli, G., Black, D.L., and Smale, S.T. (2012). Transcript dynamics of proinflammatory genes revealed by sequence analysis of subcellular RNA fractions. *Cell* **150**, 279–290.

Boija, A., Klein, I.A., Sabari, B.R., Dall'Agnesse, A., Coffey, E.L., Zamudio, A.V., Li, C.H., Shrinivas, K., Manteiga, J.C., Hannett, N.M., et al. (2018). Transcription Factors Activate Genes through the Phase-Separation Capacity of Their Activation Domains. *Cell* **175**, 1842–1855.e16.

Brescia, P., Schneider, C., Holmes, A.B., Shen, Q., Hussein, S., Pasqualucci, L., Basso, K., and Dalla-Favera, R. (2018). MEF2B Instructs Germinal Center Development and Acts as an Oncogene in B Cell Lymphomagenesis. *Cancer Cell* **34**, 453–465.e9.

Bunting, K.L., Soong, T.D., Singh, R., Jiang, Y., Béguelin, W., Poloway, D.W., Swed, B.L., Hatzl, K., Reisacher, W., Teater, M., et al. (2016). Multi-tiered Reorganization of the Genome during B Cell Affinity Maturation Anchored by a Germinal Center-Specific Locus Control Region. *Immunity* **45**, 497–512.

Calado, D.P., Sasaki, Y., Godinho, S.A., Pellerin, A., Köchert, K., Sleckman, B.P., de Alborán, I.M., Janz, M., Rodig, S., and Rajewsky, K. (2012). The cell-cycle regulator c-Myc is essential for the formation and maintenance of germinal centers. *Nat. Immunol.* **13**, 1092–1100.

Chapuy, B., McKeown, M.R., Lin, C.Y., Monti, S., Roemer, M.G.M., Qi, J., Rahl, P.B., Sun, H.H., Yeda, K.T., Doench, J.G., et al. (2013). Discovery and characterization of super-enhancer-associated dependencies in diffuse large B cell lymphoma. *Cancer Cell* **24**, 777–790.

Chen, W., Yang, Q., and Roeder, R.G. (2009). Dynamic interactions and cooperative functions of PGC-1 $\alpha$  and MED1 in TRalpha-mediated activation of the brown-fat-specific UCP-1 gene. *Mol. Cell* **35**, 755–768.

Chu, C.S., Hsu, P.H., Lo, P.W., Scheer, E., Tora, L., Tsai, H.J., Tsai, M.D., and Juan, L.J. (2011). Protein kinase A-mediated serine 35 phosphorylation dissociates histone H1.4 from mitotic chromosome. *J. Biol. Chem.* **286**, 35843–35851.

Chu, C.S., Lo, P.W., Yeh, Y.H., Hsu, P.H., Peng, S.H., Teng, Y.C., Kang, M.L., Wong, C.H., and Juan, L.J. (2014). O-GlcNAcylation regulates EZH2 protein stability and function. *Proc. Natl. Acad. Sci. USA* **111**, 1355–1360.

Corcoran, L.M., Hasbold, J., Dietrich, W., Hawkins, E., Kallies, A., Nutt, S.L., Tarlinton, D.M., Matthias, P., and Hodgkin, P.D. (2005). Differential requirement for OBF-1 during antibody-secreting cell differentiation. *J. Exp. Med.* **207**, 1385–1396.

Core, L.J., Martins, A.L., Danko, C.G., Waters, C.T., Siepel, A., and Lis, J.T. (2014). Analysis of nascent RNA identifies a unified architecture of initiation regions at mammalian promoters and enhancers. *Nat. Genet.* **46**, 1311–1320.

De Silva, N.S., and Klein, U. (2015). Dynamics of B cells in germinal centres. *Nat. Rev. Immunol.* **15**, 137–148.

Dent, A.L., Shaffer, A.L., Yu, X., Allman, D., and Staudt, L.M. (1997). Control of inflammation, cytokine expression, and germinal center formation by BCL-6. *Science* **276**, 589–592.

Dignam, J.D., Lebovitz, R.M., and Roeder, R.G. (1983). Accurate transcription initiation by RNA polymerase II in a soluble extract from isolated mammalian nuclei. *Nucleic Acids Res.* **11**, 1475–1489.

Dobin, A., Davis, C.A., Schlesinger, F., Drenkow, J., Zaleski, C., Jha, S., Batut, P., Chaisson, M., and Gingeras, T.R. (2013). STAR: ultrafast universal RNA-seq aligner. *Bioinformatics* **29**, 15–21.

Dominguez-Sola, D., Vitorica, G.D., Ying, C.Y., Phan, R.T., Saito, M., Nussenzweig, M.C., and Dalla-Favera, R. (2012). The proto-oncogene MYC is required for selection in the germinal center and cyclic reentry. *Nat. Immunol.* **13**, 1083–1091.

Duan, Z., Andronescu, M., Schutz, K., Lee, C., Shendure, J., Fields, S., Noble, W.S., and Anthony Blau, C. (2012). A genome-wide 3C-method for characterizing the three-dimensional architectures of genomes. *Methods* **58**, 277–288.

El Khattabi, L., Zhao, H., Kalchschmidt, J., Young, N., Jung, S., Van Blerkom, P., Kieffer-Kwon, P., Kieffer-Kwon, K.R., Park, S., Wang, X., et al. (2019). A Pliable Mediator Acts as a Functional Rather Than an Architectural Bridge between Promoters and Enhancers. *Cell* **178**, 1145–1158.e20.

Fukuda, T., Yoshida, T., Okada, S., Hatano, M., Miki, T., Ishibashi, K., Okabe, S., Koseki, H., Hirotsawa, S., Taniguchi, M., et al. (1997). Disruption of the Bcl6 gene results in an impaired germinal center formation. *J. Exp. Med.* **186**, 439–448.

Hagège, H., Klous, P., Braem, C., Splinter, E., Dekker, J., Cathala, G., de Laat, W., and Forné, T. (2007). Quantitative analysis of chromosome conformation capture assays (3C-qPCR). *Nat. Protoc.* **2**, 1722–1733.

Heinz, S., Benner, C., Spann, N., Bertolino, E., Lin, Y.C., Laslo, P., Cheng, J.X., Murre, C., Singh, H., and Glass, C.K. (2010). Simple combinations of lineage-determining transcription factors prime cis-regulatory elements required for macrophage and B cell identities. *Mol. Cell* **38**, 576–589.

Hnisz, D., Shrinivas, K., Young, R.A., Chakraborty, A.K., and Sharp, P.A. (2017). A Phase Separation Model for Transcriptional Control. *Cell* **169**, 13–23.

Hodson, D.J., Shaffer, A.L., Xiao, W., Wright, G.W., Schmitz, R., Phelan, J.D., Yang, Y., Webster, D.E., Rui, L., Kohlhammer, H., et al. (2016). Regulation of normal B-cell differentiation and malignant B-cell survival by OCT2. *Proc. Natl. Acad. Sci. USA* **113**, E2039–E2046.

Horlbeck, M.A., Gilbert, L.A., Villalta, J.E., Adamson, B., Pak, R.A., Chen, Y., Fields, A.P., Park, C.Y., Corn, J.E., Kampmann, M., and Weissman, J.S. (2016). Compact and highly active next-generation libraries for CRISPR-mediated gene repression and activation. *eLife* **5**, e19760.

Huang, C., Geng, H., Boss, I., Wang, L., and Melnick, A. (2014). Cooperative transcriptional repression by BCL6 and BACH2 in germinal center B-cell differentiation. *Blood* **123**, 1012–1020.

- Iida, S., Chen, W., Nakadai, T., Ohkuma, Y., and Roeder, R.G. (2015). PRDM16 enhances nuclear receptor-dependent transcription of the brown fat-specific *Ucp1* gene through interactions with Mediator subunit MED1. *Genes Dev.* **29**, 308–321.
- Ito, M., Yuan, C.X., Okano, H.J., Darnell, R.B., and Roeder, R.G. (2000). Involvement of the TRAP220 component of the TRAP/SMCC coactivator complex in embryonic development and thyroid hormone action. *Mol. Cell* **5**, 683–693.
- Jaeger, M.G., Schwalb, B., Mackowiak, S.D., Velychko, T., Hanzl, A., Imrichova, H., Brand, M., Agerer, B., Chorn, S., Nabet, B., et al. (2020). Selective Mediator dependence of cell-type-specifying transcription. *Nat. Genet.* **52**, 719–727.
- Joung, J., Konermann, S., Gootenberg, J.S., Abudayyeh, O.O., Platt, R.J., Brigham, M.D., Sanjana, N.E., and Zhang, F. (2017). Genome-scale CRISPR-Cas9 knockout and transcriptional activation screening. *Nat. Protoc.* **12**, 828–863.
- Khan, A., and Mathelier, A. (2017). Intervene: a tool for intersection and visualization of multiple gene or genomic region sets. *BMC Bioinformatics* **18**, 287.
- Kim, U., Qin, X.F., Gong, S., Stevens, S., Luo, Y., Nussenzweig, M., and Roeder, R.G. (1996). The B-cell-specific transcription coactivator OCA-B/OBF-1/Bob-1 is essential for normal production of immunoglobulin isotypes. *Nature* **383**, 542–547.
- Kim, U., Siegel, R., Ren, X., Gunther, C.S., Gaasterland, T., and Roeder, R.G. (2003). Identification of transcription coactivator OCA-B-dependent genes involved in antigen-dependent B cell differentiation by cDNA array analyses. *Proc. Natl. Acad. Sci. USA* **100**, 8868–8873.
- Kim, S., Xu, X., Hecht, A., and Boyer, T.G. (2006). Mediator is a transducer of Wnt/beta-catenin signaling. *J. Biol. Chem.* **281**, 14066–14075.
- Lai, F., Orom, U.A., Cesaroni, M., Beringer, M., Taatjes, D.J., Blobel, G.A., and Shiekhattar, R. (2013). Activating RNAs associate with Mediator to enhance chromatin architecture and transcription. *Nature* **494**, 497–501.
- Lai, F., Gardini, A., Zhang, A., and Shiekhattar, R. (2015). Integrator mediates the biogenesis of enhancer RNAs. *Nature* **525**, 399–403.
- Langmead, B., and Salzberg, S.L. (2012). Fast gapped-read alignment with Bowtie 2. *Nat. Methods* **9**, 357–359.
- Levels, M.J., Fehres, C.M., van Baarsen, L.G.M., van Uden, N.O.P., Germar, K., O'Toole, T.G., Blijdorp, I.C.J., Semmelink, J.F., Doorenspleet, M.E., Bakker, A.Q., et al. (2019). BOB.1 controls memory B-cell fate in the germinal center reaction. *J. Autoimmun.* **101**, 131–144.
- Levine, M., Cattoglio, C., and Tjian, R. (2014). Looping back to leap forward: transcription enters a new era. *Cell* **157**, 13–25.
- Li, H., Handsaker, B., Wysoker, A., Fennell, T., Ruan, J., Homer, N., Marth, G., Abecasis, G., and Durbin, R.; 1000 Genome Project Data Processing Subgroup (2009). The Sequence Alignment/Map format and SAMtools. *Bioinformatics* **25**, 2078–2079.
- Lindner, J.M., Kayo, H., Hedlund, S., Fukuda, Y., Fukao, T., and Nielsen, P.J. (2014). Cutting edge: The transcription factor Bob1 counteracts B cell activation and regulates miR-146a in B cells. *J. Immunol.* **192**, 4483–4486.
- Lovén, J., Hoke, H.A., Lin, C.Y., Lau, A., Orlando, D.A., Vakoc, C.R., Bradner, J.E., Lee, T.I., and Young, R.A. (2013). Selective inhibition of tumor oncogenes by disruption of super-enhancers. *Cell* **153**, 320–334.
- Lu, X., Chu, C.S., Fang, T., Rayon-Estrada, V., Fang, F., Patke, A., Qian, Y., Clarke, S.H., Melnick, A.M., Zhang, Y., et al. (2019). MTA2/NuRD Regulates B Cell Development and Cooperates with OCA-B in Controlling the Pre-B to Immature B Cell Transition. *Cell Rep.* **28**, 472–485.e5.
- Luo, Y., and Roeder, R.G. (1995). Cloning, functional characterization, and mechanism of action of the B-cell-specific transcriptional coactivator OCA-B. *Mol. Cell. Biol.* **15**, 4115–4124.
- Luo, Y., Fujii, H., Gerster, T., and Roeder, R.G. (1992). A novel B cell-derived coactivator potentiates the activation of immunoglobulin promoters by octamer-binding transcription factors. *Cell* **71**, 231–241.
- Malik, S., and Roeder, R.G. (2003). Isolation and functional characterization of the TRAP/mediator complex. *Methods Enzymol.* **364**, 257–284.
- Malik, S., and Roeder, R.G. (2010). The metazoan Mediator co-activator complex as an integrative hub for transcriptional regulation. *Nat. Rev. Genet.* **11**, 761–772.
- Malik, S., and Roeder, R.G. (2016). Mediator: A Drawbridge across the Enhancer-Promoter Divide. *Mol. Cell* **64**, 433–434.
- Malik, S., Guermah, M., Yuan, C.X., Wu, W., Yamamura, S., and Roeder, R.G. (2004). Structural and functional organization of TRAP220, the TRAP/mediator subunit that is targeted by nuclear receptors. *Mol. Cell. Biol.* **24**, 8244–8254.
- Malone, C.S., and Wall, R. (2002). Bob1 (OCA-B/OBF-1) differential transactivation of the B cell-specific B29 (Ig beta) and mb-1 (Ig alpha) promoters. *J. Immunol.* **168**, 3369–3375.
- Mesin, L., Ersching, J., and Victora, G.D. (2016). Germinal Center B Cell Dynamics. *Immunity* **45**, 471–482.
- Mlynarczyk, C., Fontán, L., and Melnick, A. (2019). Germinal center-derived lymphomas: The darkest side of humoral immunity. *Immunol. Rev.* **288**, 214–239.
- Molkentin, J.D., Firulli, A.B., Black, B.L., Martin, J.F., Hustad, C.M., Copeland, N., Jenkins, N., Lyons, G., and Olson, E.N. (1996). MEF2B is a potent transactivator expressed in early myogenic lineages. *Mol. Cell. Biol.* **16**, 3814–3824.
- Morin, S., Charron, F., Robitaille, L., and Nemer, M. (2000). GATA-dependent recruitment of MEF2 proteins to target promoters. *EMBO J.* **19**, 2046–2055.
- Nielsen, P.J., Georgiev, O., Lorenz, B., and Schaffner, W. (1996). B lymphocytes are impaired in mice lacking the transcriptional co-activator Bob1/OCA-B/OBF1. *Eur. J. Immunol.* **26**, 3214–3218.
- Ou, D.S., Lee, S.B., Chu, C.S., Chang, L.H., Chung, B.C., and Juan, L.J. (2011). Transcriptional activation of endoplasmic reticulum chaperone GRP78 by HCMV IE1-72 protein. *Cell Res.* **21**, 642–653.
- Pastore, A., Jurinovic, V., Kridel, R., Hoster, E., Staiger, A.M., Szczepanowski, M., Pott, C., Kopp, N., Murakami, M., Horn, H., et al. (2015). Integration of gene mutations in risk prognostication for patients receiving first-line immunotherapy for follicular lymphoma: a retrospective analysis of a prospective clinical trial and validation in a population-based registry. *Lancet Oncol.* **16**, 1111–1122.
- Pon, J.R., and Marra, M.A. (2016). MEF2 transcription factors: developmental regulators and emerging cancer genes. *Oncotarget* **7**, 2297–2312.
- Pon, J.R., Wong, J., Saberi, S., Alder, O., Moksa, M., Grace Cheng, S.-W., Morin, G.B., Hoodless, P.A., Hirst, M., and Marra, M.A. (2015). MEF2B mutations in non-Hodgkin lymphoma dysregulate cell migration by decreasing MEF2B target gene activation. *Nat. Commun.* **6**, 7953.
- Qin, X.F., Reichlin, A., Luo, Y., Roeder, R.G., and Nussenzweig, M.C. (1998). OCA-B integrates B cell antigen receptor-, CD40L- and IL 4-mediated signals for the germinal center pathway of B cell development. *EMBO J.* **17**, 5066–5075.
- Ramachandrareddy, H., Bouska, A., Shen, Y., Ji, M., Rizzino, A., Chan, W.C., and McKeithan, T.W. (2010). BCL6 promoter interacts with far upstream sequences with greatly enhanced activating histone modifications in germinal center B cells. *Proc. Natl. Acad. Sci. USA* **107**, 11930–11935.
- Ramírez, F., Ryan, D.P., Grüning, B., Bhardwaj, V., Kilpert, F., Richter, A.S., Heyne, S., Dündar, F., and Manke, T. (2016). deepTools2: a next generation web server for deep-sequencing data analysis. *Nucleic Acids Res.* **44** (W1), W160–5.
- Ren, X., Siegel, R., Kim, U., and Roeder, R.G. (2011). Direct interactions of OCA-B and TFII-I regulate immunoglobulin heavy-chain gene transcription by facilitating enhancer-promoter communication. *Mol. Cell* **42**, 342–355.
- Ryan, R.J.H., Drier, Y., Whitton, H., Cotton, M.J., Kaur, J., Issner, R., Gillespie, S., Epstein, C.B., Nardi, V., Sohani, A.R., et al. (2015). Detection of Enhancer-Associated Rearrangements Reveals Mechanisms of Oncogene Dysregulation in B-cell Lymphoma. *Cancer Discov.* **5**, 1058–1071.
- Sabari, B.R., Dall'Agnese, A., Bojja, A., Klein, I.A., Coffey, E.L., Shrinivas, K., Abraham, B.J., Hannett, N.M., Zamudio, A.V., Manteiga, J.C., et al. (2018). Coactivator condensation at super-enhancers links phase separation and gene control. *Science* **361**, eaar3958.

- Sayin, I., Radtke, A.J., Vella, L.A., Jin, W., Wherry, E.J., Buggert, M., Betts, M.R., Herati, R.S., Germain, R.N., and Canaday, D.H. (2018). Spatial distribution and function of T follicular regulatory cells in human lymph nodes. *J. Exp. Med.* *215*, 1531–1542.
- Schubart, D., Rolink, A., Kosco-Vilbois, M., Botteri, F., and Matthias, P. (1996). B-cell-specific coactivator OBF-1/OCA-B/Bob1 required for immune response and germinal centre formation. *Nature* *383*, 383538a0.
- Sciuto, M.R., Warnken, U., Schnölzer, M., Valvo, C., Brunetto, L., Boe, A., Biffoni, M., Krammer, P.H., De Maria, R., and Haas, T.L. (2018). Two-Step Coimmunoprecipitation (TIP) Enables Efficient and Highly Selective Isolation of Native Protein Complexes. *Mol. Cell. Proteomics* *17*, 993–1009.
- Shrinivas, K., Sabari, B.R., Coffey, E.L., Klein, I.A., Bojja, A., Zamudio, A.V., Schuijers, J., Hannett, N.M., Sharp, P.A., Young, R.A., and Chakraborty, A.K. (2019). Enhancer Features that Drive Formation of Transcriptional Condensates. *Mol. Cell* *75*, 549–561.e7.
- Stauss, D., Brunner, C., Berberich-Siebelt, F., Höpken, U.E., Lipp, M., and Müller, G. (2016). The transcriptional coactivator Bob1 promotes the development of follicular T helper cells via Bcl6. *EMBO J.* *35*, 881–898.
- Stevens, S., Ong, J., Kim, U., Eckhardt, L.A., and Roeder, R.G. (2000). Role of OCA-B in 3'-IgH enhancer function. *J. Immunol.* *164*, 5306–5312.
- Stumpf, M., Yue, X., Schmitz, S., Luche, H., Reddy, J.K., and Borggrefe, T. (2010). Specific erythroid-lineage defect in mice conditionally deficient for Mediator subunit Med1. *Proc. Natl. Acad. Sci. USA* *107*, 21541–21546.
- Thomas-Claudepierre, A.-S., Robert, I., Rocha, P.P., Raviram, R., Schiavo, E., Heyer, V., Bonneau, R., Luo, V.M., Reddy, J.K., Borggrefe, T., et al. (2016). Mediator facilitates transcriptional activation and dynamic long-range contacts at the IgH locus during class switch recombination. *J. Exp. Med.* *213*, 303–312.
- Wang, D., Garcia-Bassets, I., Benner, C., Li, W., Su, X., Zhou, Y., Qiu, J., Liu, W., Kaikkonen, M.U., Ohgi, K.A., et al. (2011). Reprogramming transcription by distinct classes of enhancers functionally defined by eRNA. *Nature* *474*, 390–394.
- Wang, T., Wei, J.J., Sabatini, D.M., and Lander, E.S. (2014). Genetic screens in human cells using the CRISPR-Cas9 system. *Science* *343*, 80–84.
- Weinstein, J.S., Lezon-Geyda, K., Maksimova, Y., Craft, S., Zhang, Y., Su, M., Schulz, V.P., Craft, J., and Gallagher, P.G. (2014). Global transcriptome analysis and enhancer landscape of human primary T follicular helper and T effector lymphocytes. *Blood* *124*, 3719–3729.
- Whyte, W.A., Orlando, D.A., Hnisz, D., Abraham, B.J., Lin, C.Y., Kagey, M.H., Rahl, P.B., Lee, T.I., and Young, R.A. (2013). Master transcription factors and mediator establish super-enhancers at key cell identity genes. *Cell* *153*, 307–319.
- Wolf, I., Pevzner, V., Kaiser, E., Bernhardt, G., Claudio, E., Siebenlist, U., Förster, R., and Lipp, M. (1998). Downstream activation of a TATA-less promoter by Oct-2, Bob1, and NF-kappaB directs expression of the homing receptor BLR1 to mature B cells. *J. Biol. Chem.* *273*, 28831–28836.
- Ye, B.H., Cattoretti, G., Shen, Q., Zhang, J., Hawe, N., de Waard, R., Leung, C., Nouri-Shirazi, M., Orazi, A., Chaganti, R.S., et al. (1997). The BCL-6 proto-oncogene controls germinal-centre formation and Th2-type inflammation. *Nat. Genet.* *16*, 161–170.
- Ying, C.Y., Dominguez-Sola, D., Fabi, M., Lorenz, I.C., Hussein, S., Bansal, M., Califano, A., Pasqualucci, L., Basso, K., and Dalla-Favera, R. (2013). MEF2B mutations lead to deregulated expression of the oncogene BCL6 in diffuse large B cell lymphoma. *Nat. Immunol.* *14*, 1084–1092.
- Yu, M., Yang, W., Ni, T., Tang, Z., Nakadai, T., Zhu, J., and Roeder, R.G. (2015). RNA polymerase II-associated factor 1 regulates the release and phosphorylation of paused RNA polymerase II. *Science* *350*, 1383–1386.
- Zhang, Y., Liu, T., Meyer, C.A., Eeckhoutte, J., Johnson, D.S., Bernstein, B.E., Nusbaum, C., Myers, R.M., Brown, M., Li, W., and Liu, X.S. (2008). Model-based analysis of ChIP-Seq (MACS). *Genome Biol.* *9*, R137.

STAR★METHODS

KEY RESOURCES TABLE

REAGENT or RESOURCE	SOURCE	IDENTIFIER
<b>Antibodies</b>		
IgG Fraction Monoclonal mouse Anti-rabbit IgG, light chain specific, Horseradish Peroxidase	Jackson ImmunoResearch	Cat# 211-032-171; RRID: AB_2339149
Monoclonal Anti-Biotin-Agarose	Sigma-Aldrich	Cat# A1559; RRID: AB_257936
TrueBlot anti-mouse Ig IP agarose beads	Rockland	Cat# 00-8811-25; RRID: AB_2610704
TrueBlot anti-rabbit Ig IP agarose beads	Rockland	Cat# 00-8800-25; RRID: AB_2610703
Goat anti-mouse IgG (H+L), superclonal recombinant secondary antibody, biotin	Thermo Fisher	Cat# A28176; RRID: AB_2536162
Goat anti-rabbit IgG (H+L), superclonal recombinant secondary antibody, biotin	Thermo Fisher	Cat# A27035; RRID: AB_2536098
Anti-FLAG M2 Affinity gel	Millipore Sigma	Cat# A2220
Anti-Bob1 (OCA-B), rabbit polyclonal	Santa Cruz Biotechnology	Cat# sc-955; RRID: AB_2166917
Anti-Oct-2 (OCT2), rabbit polyclonal	Santa Cruz Biotechnology	Cat# sc-233; RRID: AB_2167205
Normal rabbit IgG	Santa Cruz Biotechnology	Cat# sc-2027; RRID: AB_737197
Normal mouse IgG	Santa Cruz Biotechnology	Cat# sc-2025; RRID: AB_737182
Anti-BOB1 (OCA-B), rabbit monoclonal	Abcam	Cat# ab92315; RRID: AB_10562774
Anti-Oct-1 (OCT1), rabbit polyclonal	Santa Cruz Biotechnology	Cat# sc-232; RRID: AB_2167065
Anti-MED1, rabbit polyclonal	Bethyl	Cat# A300-793A; RRID: AB_577241
Anti-Lamin B, goat polyclonal	Santa Cruz Biotechnology	Cat# sc-6216; RRID: AB_648156
Anti- $\beta$ -actin, mouse monoclonal	Santa Cruz Biotechnology	Cat# sc-47778; RRID: AB_626632
Anti-H3K27ac, rabbit polyclonal	Abcam	Cat# ab4729; RRID: AB_2118291
Anti-EP300, rabbit polyclonal	Santa Cruz Biotechnology	Cat# sc-584; RRID: AB_2293429
Anti-CREBBP, rabbit polyclonal	Santa Cruz Biotechnology	Cat# sc-583; RRID: AB_2245237
Anti-BCL6, mouse monoclonal	Santa Cruz Biotechnology	Cat# sc-7388; RRID: AB_2063455
Anti-FLAG, mouse monoclonal	Sigma-Aldrich	Cat# F1804; RRID: AB_262044
Anti-GST, mouse monoclonal	Santa Cruz Biotechnology	Cat# sc-138; RRID: AB_627677
Anti-MED6, rabbit polyclonal	Santa Cruz Biotechnology	Cat# sc-9434; RRID: AB_2250535
Anti-RPB1, rabbit polyclonal	Santa Cruz Biotechnology	Cat# sc-899; RRID: AB_632359
Anti-OCT2, mouse monoclonal	Santa Cruz Biotechnology	Cat# sc-377476; RRID: NA
Anti-MEF2B, mouse monoclonal	Santa Cruz Biotechnology	Cat# sc-517433; RRID: NA
Anti-MEF2B, rabbit polyclonal	Sigma-Aldrich	Cat# HPA004734; RRID: AB_10963939
APC-conjugated anti-B220	BD Bioscience	Cat# 553092
PE-conjugated anti-FAS	BD Bioscience	Cat# 554258
FITC-conjugated anti-GL7	BD Bioscience	Cat# 553666
Anti-MED30, rabbit polyclonal	This lab	N/A
Anti-MED17, rabbit polyclonal	This lab	N/A
Anti-MED21, rabbit polyclonal	This lab	N/A
Anti-MED23, rabbit polyclonal	This lab	N/A
Anti-MED24, rabbit polyclonal	This lab	N/A
Anti-MED12, rabbit polyclonal	This lab	N/A
Anti-MED13, rabbit polyclonal	This lab	N/A
<b>Chemicals, Peptides, and Recombinant Proteins</b>		
DSG (disuccinimidyl glutarate)	ProteoChem	Cat# c1104
Bicine	Sigma	Cat# 391336
D(+)-Biotin	Sigma	Cat# 8512090005

(Continued on next page)

**Continued**

REAGENT or RESOURCE	SOURCE	IDENTIFIER
Iscove's Modified Dulbecco's Medium (1X), +L-Glutamine, + 25mM HEPES	Life technologies	Cat# 12440
Salmon sperm DNA	GE Healthcare Life Sciences	Cat# 27-4565-01
poly-deoxy-inosinic-deoxy-cytidylic acid [poly [d(I-C)]	Millipore Sigma	Cat# 10108812001
Biohyne™ B Nylon membrane	Thermo Fisher	Cat# 77016
Protease Inhibitor Cocktail Set III, EDTA-Free	Millipore	Cat# 539134
Cellfectin II	Invitrogen	Cat# 10362-100
Grace's Insect Medium (2X), supplemented	Invitrogen	Cat# 11667-037
Grace's Insect Medium, unsupplemented	Invitrogen	Cat# 11595-030
BS3 (bis(sulfosuccinimidyl)suberate)	Thermo Fisher	Cat# 21580
Benzonase® Nuclease	EMD Millipore	Cat# 70664
DMEM (Dulbecco's Modified Eagle Medium)	Thermo Fisher	Cat# 11960-044
Formaldehyde	Polysciences	Cat# 18814-10
TransIT-LT1	Mirus Bio LLC	Cat# MIR 2306
Opti-MEM I Reduced Serum Medium	Thermo Fisher	Cat# 31985-070
Penicillin-Streptomycin	Thermo Fisher	Cat# 15140122
Proteinase K	Roche	Cat# 3115836001
Puromycin	Life Technologies	Cat# A11138-03
Alt-R S.p. Cas9 Nuclease 3NLS	IDT	Cat# 1074182
Alt-R CRISPR-Cas0 tracrRNA	IDT	Cat# 1072532
Alt-R CRISPR-Cas9 crRNA (targeting <i>MEF2B</i> )	IDT	N/A
Alt-R CRISPR-Cas9 crRNA (targeting <i>Pou2af1</i> )	IDT	N/A
TRLzol reagent	Invitrogen	Cat# 15596026
dithiobis(succinimidyl propionate) (DSP)	Thermo Fisher	Cat# 22586
DAPI (4',6-Diamidino-2-Phenylindole, Dilactate)	Life Technologies	Cat# D3571
Glutathione Sepharose® 4B	Millipore Sigma	Cat# GE17-0756-01
Dynabeads™ Protein A	Invitrogen	Cat# 10002D
Dynabeads M-280 Streptavidin	Invitrogen	Cat# 11205D
Dynabeads™ Protein G	Invitrogen	Cat# 10003D
<b>Critical Commercial Assays</b>		
RNeasy® Plus mini kit	QIAGEN	Cat# 74034
RNase-Free DNase Set	QIAGEN	Cat# 79254
SuperScript III Reverse Transcriptase	Thermo Fisher	Cat# 18080-044
QuantiTect SYBR Green PCR mix	QIAGEN	Cat# 204143
Dual-Luciferase® Reporter Assay System	Promega	Cat# E1910
End-It™ End-Repair Kit	Epicenter	Cat# ER81050
3' → 5' exo <sup>-</sup> Klenow Fragment	NEB	Cat# M0212S
Quick Ligation Kit	NEB	Cat# M2200S
DNA Clean & Concentrator Kit	Zymo Research	Cat# D4014
NEXTflex ChIP-Seq Barcodes - 12	PerkinElmer	Cat# NOVA-514121
Phusion® High-Fidelity DNA Polymerase	NEB	Cat# M0530S
TruSeq Stranded mRNA Library Prep Kit	Illumina	Cat# 20020594
LightShift Chemiluminescent EMSA kit	Thermo Fisher	Cat# 20148
Chemiluminescent Nucleic Acid Detection Module Kit	Thermo Fisher	Cat# 89880
Taqman Universal PCR Master Mix	Applied biosystems	Cat# 4326708
Lenti-X	Takara	Cat# 631232

(Continued on next page)

**Continued**

REAGENT or RESOURCE	SOURCE	IDENTIFIER
In-Fusion HD Cloning Kit	Clontech	Cat# 639648
Restore Plus Western Blot Stripping Buffer	Thermo fisher	Cat# 46430
Amaxa SF Cell Line 96-well Nucleofector Kit	Lonza	Cat# V4SC-2096
Verso cDNA Synthesis Kit	Thermo Fisher	Cat# AB1453B
FAST SYBR Green Master Mix	Applied Biosystems	Cat# 4385614
BuccalAmp DNA Extraction Kit	Epicenter	Cat# QE09050
<b>Deposited Data</b>		
OCI-Ly7 ChIP-seq for OCA-B, OCT1, OCT2, MED1, EP300, and CREBBP (Figures 1F and S6)	This Paper	GSE133102
ChromRNA-seq (Figures S2B and S5E)	This Paper	GSE145017
SU-DHL-10 ChIP-seq for MEF2B WT (Figure S3L)	Brescia et al., 2018	GSE110682
SU-DHL-10-MEF2B-D83V ChIP-seq for MEF2B D83V (Figure S3L)	Brescia et al., 2018	GSE110682
OCI-Ly7 ChIP-seq for MEF2B (Figures 1F and S6)	Ryan et al., 2015	GSE69558
OCI-Ly7 ChIP-seq for PAX5 (Figures 1F and S6)	Ryan et al., 2015	GSE69558
OCI-Ly7 ChIP-seq for PU.1 (Figures 1F and S6)	Ryan et al., 2015	GSE69558
SU-DHL-4 ChIP-seq for MEF2B (Figures S5F and S6)	Ryan et al., 2015	GSE69558
OCI-Ly7 ChIP-seq for H3K27ac (Figure S6)	ENCODE ( <a href="https://www.encodeproject.org">https://www.encodeproject.org</a> )	ENCF787GTX
OCI-Ly7 ChIP-seq for H3K4me1 (Figure S6)	ENCODE ( <a href="https://www.encodeproject.org">https://www.encodeproject.org</a> )	ENCF583VZK
OCI-Ly7 ChIP-seq for H3K4me3 (Figure S6)	ENCODE ( <a href="https://www.encodeproject.org">https://www.encodeproject.org</a> )	ENCF852DRP
OCI-Ly7 ChIP-seq for CTCF (Figures 1F and S6)	ENCODE ( <a href="https://www.encodeproject.org">https://www.encodeproject.org</a> )	ENCF455RLT
OCI-Ly7 DNase-seq (Figures 1F and S6)	ENCODE ( <a href="https://www.encodeproject.org">https://www.encodeproject.org</a> )	ENCF506FHA
Naive B (NB) ChIP-seq for H3K27ac (Figures 1F and S6)	BLUEPRINT EPIGENOME ( <a href="https://www.blueprint-epigenome.eu">https://www.blueprint-epigenome.eu</a> )	Sample: S0138VH1 Experiment: ERX1007380
Germinal Center B (GC B) ChIP-seq for H3K27ac (Figures 1F and S6)	BLUEPRINT EPIGENOME ( <a href="https://www.blueprint-epigenome.eu">https://www.blueprint-epigenome.eu</a> )	Sample: S013ARH1 Experiment: ERX1007385
<b>Experimental Models: Cell Lines</b>		
OCI-Ly7	Ontario Cancer Institute	Cat# DSMZ ACC-688, RRID: CVCL_1881
SU-DHL-4	ATCC	Cat# ATCC CRL-2957, RRID: CVCL_0539
293T	ATCC	Cat# CRL-3216, RRID: CVCL_0063
SF9	ATCC	Cat# CRL-1711, RRID: CVCL_0549
Mouse embryonic fibroblast	Ito et al., 2000	N/A
Mouse embryonic fibroblast: MED1 <sup>-/-</sup>	Ito et al., 2000	N/A
<b>Experimental Models: Organisms/Strains</b>		
Mouse: C57BL/6J	The Jackson Laboratory	Cat# JAX:000664
Mouse: <i>Bcl6</i> <sup>-/-</sup>	H. Ye, Albert Einstein Medical College; Ye et al., 1997	N/A
Mouse: <i>Bcl6</i> LCR <sup>-/-</sup>	Bunting et al., 2016	N/A
<b>Oligonucleotides</b>		
Primers for RT-QPCR	This paper	Table S3
Primers for ChIP-QPCR	This paper	Table S3

(Continued on next page)

**Continued**

REAGENT or RESOURCE	SOURCE	IDENTIFIER
Primers for 3C-QPCR	This paper and Ramachandrareddy et al., 2010	Table S3
Primers for sequencing library PCR	Joung et al., 2017	Table S4
Primers for CRISPR-mediated editing on human genome	This paper	Table S5
Oligonucleotides for DNA binding assays	This paper	Table S6
Oligonucleotides for shRNA-mediated knockdown	Lu et al., 2019	Table S5
<b>Recombinant DNA</b>		
pLKO.1 scramble shRNA	Sigma-Aldrich	Cat# SHC002
pLKO.1 sh_hOCA-B	Lu et al., 2019	N/A
psPAX2	Addgene	Cat# 12260
pMD2.G	Addgene	Cat# 12259
lentiCRISPR v2	Addgene	Cat# 52961
lentiCas9-Blast	Addgene	Cat# 52962
pFUGW-pCMV-FLAG-OCA-B	This paper	N/A
pFUGW-pCMV-FLAG-OCT2	This paper	N/A
pFUGW-pCMV-FLAG-MEF2B	This paper	N/A
pGL3.basic	Promega	Cat# E1751
pRL-CMV	Promega	Cat# E2261
pGL3-Igh	Ren et al., 2011	N/A
pGL3-Igh-CE1_O2-4	This paper	N/A
pGL3-Igh-CE1_O2-4_mO3	This paper	N/A
pTO-FLAG-MED1	Iida et al., 2015	N/A
pTO-FLAG-OCA-B	This paper	N/A
pTO-FLAG-OCT2	This paper	N/A
pFBV-FLAG-MEF2B	This paper	N/A
pFBV-FLAG-MEF2B-Y69H-D83V	This paper	N/A
pTO-GST-OCA-B	This paper	N/A
pTO-GST	This paper	N/A
pGL3-CE1_O1-4	This paper	N/A
pGL3-CE1_O1-3	This paper	N/A
pGL3-CE1_O1-2	This paper	N/A
pGL3-CE1_O1	This paper	N/A
pHR-SFFV-dCas9-BFP-KRAB	Addgene	Cat# 46911
pLKO.5.C+E.sgRNA.EFS.PAC	This paper	N/A
pLKO.5.C+E.sgRNA.EFS.GFP	This paper	N/A
<b>Biological samples</b>		
Sheep red blood cells	Cocalico Biologicals	Cat# 20-1334A
<b>Software and Algorithms</b>		
STAR	Dobin et al., 2013	<a href="https://github.com/alexdobin/STAR">https://github.com/alexdobin/STAR</a>
Bowtie2	Langmead and Salzberg, 2012	<a href="http://bowtie-bio.sourceforge.net/bowtie2/index.shtml">http://bowtie-bio.sourceforge.net/bowtie2/index.shtml</a>
Samtools	Li et al., 2009	<a href="http://samtools.sourceforge.net/">http://samtools.sourceforge.net/</a>
MACS2	Zhang et al., 2008	<a href="https://github.com/mac3-project/MACS">https://github.com/mac3-project/MACS</a>
deepTools2	Ramírez et al., 2016	<a href="https://deeptools.readthedocs.io/en/develop/">https://deeptools.readthedocs.io/en/develop/</a>
Homer	Heinz et al., 2010	<a href="http://homer.ucsd.edu/homer/">http://homer.ucsd.edu/homer/</a>
Intervene	Khan and Mathelier, 2017	<a href="https://intervene.readthedocs.io/en/latest/">https://intervene.readthedocs.io/en/latest/</a>

(Continued on next page)

**Continued**

REAGENT or RESOURCE	SOURCE	IDENTIFIER
TFBSTools v1.22	N/A	<a href="http://bioconductor.org/packages/release/bioc/html/TFBSTools.html">http://bioconductor.org/packages/release/bioc/html/TFBSTools.html</a>
universalmotif v1.2.1	N/A	<a href="https://github.com/bjmt/universalmotif">https://github.com/bjmt/universalmotif</a>

**RESOURCE AVAILABILITY**

**Lead Contact**

Further information and requests for resources and reagents should be directed to and will be fulfilled by the lead contact, Robert G. Roeder ([roeder@rockefeller.edu](mailto:roeder@rockefeller.edu)).

**Materials Availability**

Unique and stable reagents generated in this study are available upon request.

**Data and Code Availability**

Complete and annotated code including gRNA library design, CRISPRi screening analysis, transcription factor motif analysis and R-based FACS and statistics analysis are available at <https://jchellmuth.com/code/>. All genomics data in this paper are available at the NCBI Gene Expression Omnibus under accession numbers GSE133102 for ChIP-seq and GSE145017 for ChromRNA-seq. A UCSC track hub to fully explore all relevant data at the *BCL6* locus is available through <https://jchellmuth.com/code/>.

**EXPERIMENTAL MODEL AND SUBJECT DETAILS**

**Cell Lines**

Human DLBCL cell lines were grown in medium containing either 90% Iscove's Modified Dulbecco's Medium (12440053, Thermo Fisher Scientific) with 20% FBS (OCI-Ly7) or 90% RPMI-1640 (11875085, Thermo Fisher Scientific) with 10% FBS (SU-DHL-4), each supplemented with 1% glutamine, and 1% penicillin/streptomycin (15140122, Thermo Fisher Scientific). OCI-Ly7 were obtained from Ontario Cancer Institute in June 2011. SU-DHL-4 cells were obtained from ATCC (CRL-2957).

HEK293T (CRL-3216, ATCC) cells were cultured in complete DMEM (11995040, Thermo Fisher Scientific) supplemented with 10% FCS and 100 U/mL PenStrep (15140122, Thermo Fisher Scientific).

**Mouse Models and Strains**

*Bcl6*<sup>-/-</sup> mice were kindly provided by H. Ye (Albert Einstein Medical College). *Bcl6* LCR<sup>-/-</sup> mice were generated in our lab as reported previously (Bunting et al., 2016). Mice were crossed as indicated in Figure 5A to generate trans double heterozygous *Bcl6*<sup>+/-</sup> LCR<sup>+/-</sup> mice and control genotypes. Mice of each genotype were matched as closely as possible for age and sex within constraints of availability (WT: n = 10, female:male = 10:0, median age = 79 ± 0 days.; *Bcl6*<sup>-/+</sup>;LCR<sup>+/+</sup>: n = 8, female:male = 4:4, median age = 103 ± 12 days; *Bcl6*<sup>+/+</sup>;LCR<sup>+/-</sup>: n = 11, female:male = 3:8, median age = 97 ± 12 days; *Bcl6*<sup>+/+</sup>;LCR<sup>-/-</sup>: n = 11, female:male = 9:2, median age = 119 ± 37.6 days; *Bcl6*<sup>-/+</sup>;LCR<sup>+/-</sup>: n = 8, female:male = 6:2, median age = 124 ± 9.32 days). Mice were housed in a dedicated pathogen-free environment. All experiments and procedures conformed to ethical principles and guidelines revised and approved by the Research Animal Resource Center of the Weill Cornell Medical College of Medicine. The use of human tissue was approved by the research ethics board of Weill Cornell Medical Center.

**METHOD DETAILS**

**Crosslinked Chromatin Immunoprecipitation (ChIP) and ChIP-sequencing**

ChIP-seq was performed as described (Yu et al., 2015) with the following modifications. Briefly, 2 × 10<sup>7</sup> cells were fixed with 1% formaldehyde for 10 min at room temperature after 45 min of incubation with DSG. Fragmentation of fixed chromatin was performed by sonication of isolated nuclei (Branson Sonifiers, Branson) to achieve enrichment of short chromatin fragments (200 - 700 bp). Five μg of antibodies were added to the chromatin lysate and incubated overnight at 4°C. The next day, Dynabeads protein A (10002D, Thermo Fisher Scientific) was added and incubated with rotation at 4°C for 1.5 hours. Enriched DNA was isolated through extensive wash steps and subsequent reverse cross-linking and purification by DNA Clean & Concentrator Kit (D4014, Zymo Research). Quantitative ChIP PCR were performed using QuantiTect SYBR Green PCR Kit (204143, QIAGEN) in 20 μL reactions with 200 pg of DNA and primers (Table S3) used at a final concentration of 0.5 μM on Applied Biosystems 7300 Real-Time PCR System (ThermoFisher). ChIP-seq libraries were prepared from 2-5 ng ChIP DNA. After end-repair (End-It™ End-Repair Kit, ER0720, Lucigen), A-tailing (3' → 5' exo<sup>-</sup> Klenow Fragment, M0212S, NEB), and ligation (Quick Ligation Kit, M2200S, NEB) with barcodes (NEXTflexChIP-Seq Barc-

odes, PerkinElmer #NOVA-514121), barcoded DNA was amplified by 12 cycles of PCR using Phusion® High-Fidelity DNA Polymerase (M0530S, NEB). Libraries were then sequenced on Illumina HiSeq 2500 as 50-bp single-end runs at the Genomics Resource Center at the Rockefeller University. The antibodies used for ChIP are described in Key Resource Table.

### Data analysis for ChIP-seq

ChIP-seq analyses for [Figures 1A–1E](#) and [S1](#) were performed as described with modifications ([Lu et al., 2019](#)). In brief, sequencing data were aligned to human hg38 reference genome using Bowtie2 ([Langmead and Salzberg, 2012](#); Galaxy Version 2.3.4.2) with default parameters. Duplicate mapped reads were removed using Samtools with the rmdup option ([Li et al., 2009](#); Galaxy Version 2.0.1). Metaplots for ChIP-seq signals were plotted as averaged profiles or heatmaps by deepTools2 ([Ramírez et al., 2016](#)). Peaks were defined by Homer ([Heinz et al., 2010](#)) using the findPeaks program with parameter -style factor and the threshold for statistical significance of peaks at  $10^{-9}$ . Filtered peaks were annotated, and genomic distributions of filtered peaks were calculated by Homer with annotatePeaks program. Measurement of peak overlap was done by Intervene ([Khan and Mathelier, 2017](#)) with default parameters. De novo motif analysis was performed with homer findMotifsGenome.pl with the following parameters: '-size 50 -bits' and the JASPAR CORE database (2020 release). For the analysis of MEF2B ChIP-seq data, MACS2 was used to identify peaks using the default settings. MEF2B peaks co-bound by OCT2 and OCAB were identified using the ChIPseeker package and the relative fraction of peaks was calculated by comparing the fraction of co-bound peaks to all peaks. The softwares used for ChIP-seq data analyses are listed in Key Resources Table.

### Lentivirus Production, Transduction, and shRNA-Mediated Gene Knock-down

Production of lentiviruses bearing lentiviral vectors and transduction of lentiviruses were performed as described by The RNAi Consortium (TRC). In brief, the day before transduction, HEK293T cells were seeded at the density of  $4 \times 10^6$  of cells in a 10-cm dish. The next day, 50  $\mu$ L of virus concentrated using Lenti-X (631232, Takara) were added to cells with complete medium containing 8  $\mu$ g/mL polybrene. The next day, cells were replenished with fresh complete medium. Positively transduced cells were selected by treating with puromycin at the final concentration of 1 mg/mL for 2 days following 2 days of transduction. For lentivirus-mediated gene knock-down,  $4 \times 10^6$  of cells were transduced by 50  $\mu$ L of virus concentrated using Lenti-X (631232, Takara) with complete medium containing 8  $\mu$ g/mL polybrene. The next day, cells were replenished with fresh complete medium. Positively transduced cells were selected by treating with puromycin at the final concentration of 1 mg/mL for 2 days following 2 days of transduction before harvest. pLKO.1 clones containing control shRNA (shCTRL) or shRNA against OCA-B mRNA (shOCA-B) are purchased from Sigma. shOCA-B has been used and validated as described ([Chapuy et al., 2013](#)). The shRNA sequences are listed in [Table S5](#) and [Key Resources Table](#).

### CRISPR/Cas9-mediated Gene Editing

For *POU2AF1*<sup>-/-</sup> and *MEF2B*<sup>-/-</sup> cells, Cas9/RNP complex containing Alt-R S.p. Cas9 Nuclease 3NLS (1074182, IDT), Alt-R CRISPR-Cas9 crRNA for *MEF2B* and *POU2AF1* (designed and synthesized by IDT), and Alt-R CRISPR-Cas9 tracrRNA (1072532, IDT) were assembled *in vitro* following manufacturer's instruction (IDT) and delivered into OCI-Ly7 cells by electroporation using Amaxa SF Cell Line 96-well Nucleofector Kit (Lonza). Single cells were then seeded in 96-well plates by serial dilution. Clones were expanded and validated by Sanger sequencing and immunoblot.

For *POU2F2*<sup>-/-</sup>, *CE1*<sup>-/-</sup>, and *CE1*<sup>+/-</sup> cells, gRNA sequences were cloned into lentiCRISPR v2 (52961, Addgene). Lentivirus production and transduction was performed as described above. Infected and selected single cells were then seeded in 96-well plates by serial dilution. Of note, *CE1* deleted cells were generated by dual transduction of two gRNAs targeting each side of *CE1* peak spanning ~200 bp. Clones were expanded and validated by Sanger sequencing and immunoblot. gRNA sequences are listed in [Table S5](#).

### Generation of CRISPRi Cell Lines

CRISPRi OCI-Ly7 and SU-DHL-4 cell lines were generated by lentiviral transduction of pHR-SFFV-dCas9-BFP-KRAB (46911, Addgene, a gift from Stanley Qi and Jonathan Weissman) followed by flow sorting for BFP high populations. Cells were expanded and sorted again after 1-2 weeks. Flow sorting was repeated 2-3 times.

### CRISPRi-mediated interference

Individual gRNA oligos were ordered from IDT and cloned into pLKO5.C+E.sgRNA.EFS.PAC for qPCR experiments or pLKO5.C+E.sgRNA.EFS.GFP for drop-out experiments. gRNA sequences are listed in [Table S5](#). gRNA constructs were lentivirally transduced into OCI-Ly7 or SU-DHL-4 CRISPRi cell lines. For CRISPRi followed by qPCR, puromycin selection was initiated 2 days after transduction. After two days of puro selection, cells were harvested and transcripts were measure by RT-qPCR (see below). For CRISPRi followed by drop-out analysis, see below ([CRISPRi Screen Validation Experiments](#)).

### RNA Isolation, cDNA preparation, and Quantitative real-time PCR (qPCR)

For experiments in [Figures 2](#) and [6](#), total RNA was prepared using TRIzol reagent (Invitrogen) following the manufacturer's protocol. cDNA was synthesized with the Verso cDNA Synthesis Kit (Thermo Scientific) using a 3:1 mix of random hexamers and

anchored oligo-dT primers. Quantitative PCR was performed using the FAST SYBR Green Master Mix (Applied Biosystems) on a QuantStudio 6 Real-Time PCR System (Applied Biosystems). For experiments in [Figure 5](#), total RNA from  $1 \times 10^6$  of CRISPR/Cas9-edited cells were prepared using RNeasy® Plus mini kit (74034, QIAGEN) with on-column digestion (RNase-Free DNase Set, 79254, QIAGEN) following manufacturer's instruction. The concentration of eluted total RNA was measured by Nanodrop (ThermoFisher). cDNAs were synthesized from 3  $\mu$ g total RNA using SuperScript III Reverse Transcriptase (18080-044, ThermoFisher) with oligo(dT) primers following manufacturer's instructions. Quantitative PCR was performed using QuantiTect SYBR Green PCR Kit (204143, QIAGEN) on Applied Biosystems 7300 Real-Time PCR System. We normalized gene expression to *HPRT1* or *TBP* and expressed values relative to control using the  $\Delta\Delta$ CT method. Primers used here are listed in [Table S3](#). Error bars represent mean  $\pm$  SD ( $n = 3$ ).

### Luciferase Assay

Luciferase assays were performed using Dual-Luciferase® Reporter Assay System (E1910, Promega) as described ([Ou et al., 2011](#)) with modifications. In brief, HEK293T cells were transfected with pGL3-*Ighluc*-CE1\_O2-O4 or pGL3-*Ighluc*-CE1\_O2-O4\_O3mut, pRL-CMV (Promega), and pFUGW-pCMV-driven *POU2F2*, *POU2AF1*, and/or *MEF2B* ORFs using TransIT-LT1 transfection reagent (MIR 2306, Mirus Bio LLC). After 24 hours, cells were washed with PBS once, harvested with 1X PLB buffer, and lysed by passive lysis. Debris was cleared by centrifugation at 14,000 rpm for 15 min and 20  $\mu$ L of the supernatant was added to 100  $\mu$ L of LAR II to measure firefly luciferase activity by TROPIX luminometer (PerkinElmer). Renilla luciferase activity was measured by adding 100  $\mu$ L of STOP & Glo Reagent. Relative luciferase activity was calculated by first normalizing firefly luciferase activity with Renilla luciferase activity, followed by dividing each group to EV. Error bars represent mean  $\pm$  SEM ( $n = 3$ ). pFUGW-pCMV-related vectors are modified from lentiCas9-Blast (52962, Addgene) and ORFs were inserted by using AgeI and BamHI sites. Sequences of the inserted CE1 fragments are listed in the [Table S6](#).

### Immunoprecipitation and Immunoprecipitation Mass Spectrometry (IP-MS)

For IP-MS, 200  $\mu$ L DynaBeads protein A (10001D, ThermoFisher) were washed twice with 1 mL washing Buffer PBST (PBS containing 0.05% Tween-20) and 20  $\mu$ g of anti-OCA-B antibodies or normal rabbit antibodies were added and incubated with beads for 6 h. Beads were washed twice with PBST. Crosslinking was performed by adding bis(sulfosuccinimidyl)suberate (BS3, 21580, ThermoFisher) at a final concentration of 5 mM in TBST and incubating for 1 h at room temperature. Beads were washed twice with PBST, quenched by adding Tris-HCl, pH 7.4 at final concentration of 50 mM, and incubated for 15 min at room temperature. Beads were mixed with 50 mg of nuclear extract from OCI-Ly7 in BC200 buffer (20 mM Tris-HCl at pH 7.5, 200 mM KCl, 10% glycerol, 0.2 mM EDTA, 3 mg/mL BSA, 0.5 mM DTT, 0.5 mM PMSF, 0.1% NP-40) and incubated overnight. Beads were washed five times with BC200 buffer and eluted with 200  $\mu$ L of 100 mM glycine, pH 2.5, with immediate neutralization by 1/10 volume of 1 M Tris-HCl, pH 8.0. Eluents were desalted by Amicon Ultra Centrifuge Filters with 10 kDa NMWCO (UFC500308, Millipore-Sigma) and sent for mass spectrometry analysis by the Rockefeller Proteomic Facility with Trypin digestion. Summary for the selected peptides acquired from mass spectrometry are listed in [Table S1](#). Co-immunoprecipitation assays of endogenous proteins in nuclear extract from OCI-Ly7 were performed as described ([Chu et al., 2014](#)). Two-Step Coimmunoprecipitation was performed as described with modifications ([Sciuto et al., 2018](#)). In brief, nuclear extracts were first incubated with rabbit anti-OCA-B antibody for IP (see scheme in [Figure S2D](#)) followed by addition of biotin-conjugated anti-rabbit IgG antibody and anti-biotin beads to immobilized proteins associated with OCA-B. After elution with excess biotin in biotin elution buffer (10 mM Tris-HCl pH 7.5, 3.3 mM biotin, 3.3 mM bicine, 120 mM NaCl, 2 mM KCl, 0.5 mM EDTA, 0.5% NP40, protease inhibitor cocktail), the eluent were incubated with mouse anti-OCT2 antibody followed by addition of biotin-conjugated anti-mouse IgG antibody and anti-mouse IgG beads to immobilized proteins associated with OCT2. After washing 6 times, the beads were boiled in  $1 \times$  Laemmli sample buffer, separated by SDS-PAGE, and analyzed by immunoblot using indicated primary antibodies and light-chain specific secondary antibody (Jackson ImmunoResearch).

### Purification of Recombinant Proteins

GST-fused OCA-B (GST-OCA-B), Flag-tagged OCT2 (F:OCT2), F:OCA-B, and F:MEFB proteins were cloned in Bac-to-Bac baculovirus expression system (Invitrogen), expressed in Sf9 cells and purified by immobilizing on Glutathione Sepharose® 4B (GE17-0756-01, Millipore Sigma) or by using Anti-FLAG M2 Affinity gel (A2220, Millipore Sigma). Recombinant F:MED1 was expressed and purified as described ([Iida et al., 2015](#)). All recombinant proteins were stored in BC buffer (20 mM Tris-HCl [pH 7.9], 20% glycerol, 0.1 mM EDTA [pH 8.0]) containing 100 mM KCl (BC100).

### Purification of the Mediator Complex from HeLa

Nuclear extracts were prepared as described ([Dignam et al., 1983](#)) from a HeLa-derived cell line that stably expresses a FLAG-tagged human MED10. Mediator complex in the nuclear extract was first enriched by a Phosphocellulose 11 anion exchange column from a 0.3–0.5 M KCl step fraction and affinity-purified by anti-FLAG M2 Affinity gel as described previously ([Malik and Roeder, 2003](#)).

### Protein-protein Interactions and Reversible Crosslinking-coupled Binding Assays

*In vitro* protein binding assays were performed as described ([Malik et al., 2004](#)). In brief, GST or GST-fused OCA-B immobilized on Glutathione Sepharose beads were incubated with either purified Mediator complex, F:MED1, F:OCT2, F:MEF2B, or nuclear extracts

from mouse embryonic fibroblasts in binding buffer (20 mM Tris-HCl at pH 7.5, 10% glycerol, 0.2 mM EDTA, 3 mg/mL BSA, 0.5 mM DTT, 0.5 mM PMSF, 0.1% NP-40) with indicated KCl concentration for 4 hours at 4°C. Beads were then washed with wash buffer (20 mM Tris-HCl at pH 7.5, 0.1 mM EDTA, 20% glycerol, 0.5 mM DTT, 0.5 mM PMSF, 0.1% NP-40) containing indicated KCl concentration for 3 times. Bound proteins were eluted by boiling in 1 × Laemmli sample buffer, separated by SDS-PAGE, and analyzed by immunoblot using indicated antibodies. Reversible crosslinking-coupled binding assay was performed as described (Kim et al., 2006) with minor modifications. Briefly, GST or GST-fused OCA-B immobilized on Glutathione Sepharose beads were incubated with purified Mediator complex, washed with binding buffer (20 mM Tris-HCl at pH 7.5, 150 mM KCl, 10% glycerol, 0.2 mM EDTA, 3 mg/mL BSA, 0.5 mM DTT, 0.5 mM PMSF, 0.1% NP-40), and crosslinked with various concentrations of dithiobis(succinimidyl propionate) (DSP, 22586, Thermo Fisher) in crosslinking buffer (20 mM HEPES [pH 7.9] and 100 mM KCl) for 10 min at room temperature. The crosslinking reaction was terminated by quenching buffer (30 mM Tris-HCl [pH 7.5] and 100 mM KCl) for 15 min and washed with washing buffer (30 mM Tris-HCl [pH 7.5], 6.0 M urea and 1% SDS) to remove uncrosslinked proteins. After crosslinking reversal by DTT at 37°C for 30 min, eluted proteins were boiled in 1 × Laemmli sample buffer, separated by SDS-PAGE, and analyzed by immunoblot using indicated antibodies.

### Immobilized Template Assay

Immobilized template assays were performed as described (Chen et al., 2009). A human *BCL6* CE1 enhancer fragment, its deletion series, or OCTA mutant was prepared by PCR using biotinylated oligonucleotides (Figure S3B and Table S6) and immobilized on streptavidin-conjugated magnetic beads (Dynabeads M280 streptavidin, Invitrogen). After incubating the beads in blocking buffer {50 mM Tris-HCl at pH 7.5, 100 mM KCl, 0.01% NP-40, 1 mg/mL BSA, 0.5 mM PMSF, 10 mM DDT, 10 μg/mL salmon sperm DNA [27-4565-01, GE Healthcare], 10 μg/mL poly-deoxy-inosinic-deoxy-cytidylic acid [poly [d(I-C)], 10108812001, Millipore Sigma]}, purified proteins were added to the reaction and incubated for 30 min at room temperature. The beads were then washed with wash buffer (50 mM Tris-HCl at pH 7.5, 100 mM KCl, 0.01% NP-40, 0.5 mM PMSF, 0.5 mM DTT) three times, and the bound proteins were eluted by boiling in 1 × Laemmli sample buffer, separated by SDS-PAGE, and analyzed by immunoblot using indicated antibodies.

### Electrophoresis Mobility Shift Assay (EMSA)

Protein-DNA binding interactions were identified by Electrophoresis Mobility Shift Assay (EMSA) using LightShift™ Chemiluminescent EMSA Kit (20148, Thermo Fisher Scientific) as described (Chu et al., 2011) with modifications. In brief, recombinant F:OCT2, F:OCA-B, and/or F:MEF2B were mixed with the biotinylated DNA probe at room temperature for 30 min, followed by electrophoresis by a 5% native polyacrylamide gel in 0.5X tris-borate EDTA buffer at 100 V for 1 h. The DNA was then transferred onto Biodyne™ B Nylon membrane (77016, Thermo Fisher Scientific) in 0.5X Tris-borate EDTA buffer at 100 V for 1 h. DNA was further cross-linked on the blot by UV at 120 mJ/cm<sup>2</sup> (UV Stratalinker 2400, Stratagene). Detection of biotinylated DNA was performed by Chemiluminescent Nucleic Acid Detection Module Kit (89880, Thermo Fisher Scientific). For competition assays, non-biotinylated probes were used as cold probes and mixed together with the biotinylated probe prior to the addition of recombinant proteins. DNA probe sequences are listed in Table S6.

### Immunization and FACS Analysis of GC B Cells

Animals were immunized intraperitoneally at 2-4 months of age with 0.5 mL of a 2% sheep red blood cell suspension in PBS (SRBC, Cocalico Biologicals) and sacrificed 10 days later for analysis of GC formation. Splenocytes were isolated and GC B cells were analyzed by gating B220<sup>+</sup>DAPI<sup>-</sup>GL7<sup>+</sup>FAS<sup>+</sup> population using FACS and the following fluorescent-labeled antibodies: APC-conjugated B220 (553092, BD Bioscience), PE-conjugated FAS (554258, BD Biosciences), FITC-conjugated GL7 (553666, BD Biosciences). DAPI was used for the exclusion of dead cells. Data was acquired on a BD FACS Canto II flow cytometer and analyzed using FlowJo software.

### Chromosome Conformation Capture Assay (3C)

Chromosome conformation capture assay was performed as described (Hagège et al., 2007) with modifications. In brief, cells were fixed with 1% of formaldehyde for 10 min at room temperature and quenched with 125 mM of glycine for 10 min at room temperature. Fixed cells were pelleted, washed once with DPBS, resuspended in ice-cold lysis buffer, and incubated for 15 min at 4°C. The nuclei were pelleted by centrifugation for 5 min at 400 g at 4°C and resuspended in 1X NEB EcoRI buffer. SDS was added to 0.01% and the nuclei were incubated at 65°C for 10 min sharp before being quenched by adding Triton X-100 to final 0.1%. EcoRI was added and the nuclei were incubated at 37°C overnight. The next day, EcoRI was inactivated by adding excess SDS and incubated at 65°C for 30 min. *In situ* proximity ligation was performed as described (Duan et al., 2012) and incubated at 16°C for 4 hours and 25°C for one hour. Reversal of crosslinks and protein degradation were performed by adding proteinase K (3115836001, Roche) and incubated overnight at 65°C. Additional proteinase K were added and incubated for another 2 h at 65°C. DNA was purified using phenol:chloroform:isoamyl alcohol (P2069, Sigma) and precipitated by sodium acetate and cold ethanol. Quantitative PCR was performed anchoring at *BCL6* promoter toward the LCR using primers as partly described (Ramachandrareddy et al., 2010) and listed in Table S3. Relative interaction frequency was calculated by normalized with that of *EEF1G* locus (Ramachandrareddy et al., 2010).

### gRNA Library Design

The regions targeted by the library consisted of all potential regulatory elements at the human *BCL6* locus including the entire *BCL6* LCR, adjacent enhancers, the *BCL6* promoter and the three alternative promoters for the next upstream coding gene (*LPP*) as well as ample interspersed genomic regions without evidence of regulatory potential as negative controls. To construct a gRNA library tiling the *BCL6* locus at the highest possible density we used custom R code. Briefly, all potential PAM sequences (NGG) and the corresponding 20bp protospacer sequence were identified in the targeted regions. All gRNAs with potential termination signals (TTTT) were removed as well as polyA/C/G stretches (AAAAA, GGGGG, CCCCC) to avoid synthesis and sequencing errors. gRNA with Esp3I sites were removed to avoid cloning errors. gRNA that showed > 1 perfect off-target matches were removed.

We selected the top 100 essential genes from two published genome-wide screens (Horlbeck et al., 2016; Wang et al., 2014) and included five CRISPRi gRNAs per essential gene into the library as positive. 250 non-targeting gRNAs were included as negative controls. Library gRNA sequences are provided in Table S2.

### gRNA Library Cloning

Oligos were synthesized on chip (Agilent Technologies, Inc.) and PCR amplified. Both inserts and pLKO5.C+E.sgRNA.EFS.PAC vector were digested simultaneously with Esp3I (Thermo Scientific) and ligated by T4 ligase (New England Biolabs Inc.) followed by electroporation into Endura Competent Cells (Lucigen). Colonies were collected and Maxi-prepped (QIAGEN) for Hi-seq QC analysis.

### CRISPRi Screening

CRISPR screening generally followed published protocols (Joung et al., 2017) with minor modifications. The gRNA library was packaged into lentiviral particles in HEK293T cells transfected with the gRNA library, pMD2.G (12259, Addgene) and psPAX2 (12260, Addgene) using TransIT-LT1 transfection reagent (Mirus Bio). CRISPRi expressing cells were transduced with the gRNA library at low MOI for an infection rate of approximately 20%–30%. Selection with puromycin was started 2 days after transduction. After three days of puromycin selection, cells were split and the baseline sample (time point t0) was stored as a dry cell pellet at –80°C. The remainder of cells were grown for 10–14 population doublings when the final sample was isolated (time point t14).

gDNA was isolated from t0 and t14 samples using the Quick-DNA Midiprep Plus kit (Zymo Research). Sequencing libraries were generated in a one-step PCR using the primers listed in Table S4. The forward primer contained a staggered stuffer to increase amplicon diversity. We used 9 different barcodes for the reverse primer to allow multiplexed sequencing. PCR products were concentrated using Zymo-Spin V columns (Zymo Research) and gDNA was removed by gel purification. Amplicons were sequenced on an Illumina HiSeq2500 machine.

The screen was performed in two independent replicates (CRISPRi). Library representation was 500–1000x at all steps of the screen including transduction, cell culture, gRNA isolation, library preparation and sequencing.

### CRISPRi Screen Analysis

Read counts for each gRNA were generated with the python script *count\_spacers.py* provided by Joung et al. (Joung et al., 2017). gRNAs with < 50 reads in any of the t0 libraries were removed. Growth scores for each gRNA was calculated as follows:

$$gs_x = \log_2 \left( \frac{rc_x t14}{rc_x t0} \right) - gs.correction$$
$$gs.correction = \frac{1}{N} \sum_{i=1}^N \log_2 \left( \frac{rc.control_i t14}{rc.control_i t0} \right)$$

Where  $rc_x t0$  and  $rc_x t14$  are the read counts at time point t0 and t14, respectively, and  $gs_x$  is the growth score of an individual gRNA. A growth score correction (*gs.correction*) representing the mean log2-fold change of all control gRNAs is subtracted to account for a negative fold-change bias introduced by normalization. For the sliding window calculation, the mean growth score of all gRNAs in each 200 bp window was calculated and mapped to the midpoint of each window. Custom code detailing screen analysis is provided. gRNA read counts and growth scores are provided in Table S2.

### CRISPRi Screen Validation Experiments

Individual gRNA oligos were ordered from IDT and cloned into pLKO5.C+E.sgRNA.EFS.GFP for drop-out experiments. Each region was independently targeted with two different gRNAs represented by two separate lines in Figures 6C and Figures S5C and S5D. Negative control (desert) regions were selected based on the absence of any activating histone marks. gRNA sequences are listed in Table S5. gRNA constructs were lentivirally transduced into OCI-Ly7 or SU-DHL-4 CRISPRi cell lines. For drop-out curves, cells were infected with GFP-tagged constructs at an infection rate of 20%–50% and the fraction of GFP positive cells was monitored by FACS every 3–4 days. The fraction of GFP positive cells was normalized to the fraction of GFP positive cells at day 3–4. Custom R code was used for analysis of FACS data and plotting of results.

### Constituent-enhancer-based Analysis

We defined constituent enhancers at the *BCL6* locus using Encode DNase-seq peaks (ENCFF328RHP). The top quartile peaks were extended to 2 kb windows. Overlapping windows and windows within < 100 bp of each other were merged. This constituent enhancer definition correlated well with other surrogate markers of enhancer activity (H3K27ac and ATAC-seq, data not shown) and functional data (CRISPRi).

To identify essential enhancers, we calculated the mean of all gRNA growth scores within each constituent enhancer. Constituent enhancers with a mean growth score smaller than the 1<sup>st</sup> percentile of all CRISPRi control gRNAs, were classified as essential enhancers.

To quantify ChIP-seq, DNase-seq and ChromRNA-seq at each constituent enhancer, we summarized read coverage and normalized for enhancer length.

### Sequencing and Analysis of Chromatin-bound RNA (ChromRNA-seq)

ChromRNA-seq was performed for three independent replicates of OCI-Ly7 cells expressing CRISPRi (dCas9-BFP-KRAB, 46911, Addgene) and a control, non-targeting gRNA. Expression of the CRISPRi system and gRNA did not noticeably alter growth rate, morphological appearance or viability. ChromRNA-seq was performed as previously described (Bhatt et al., 2012; Lai et al., 2015) with minor changes. Nuclei were isolated using the PURE Prep Nuclei Isolation Kit (NUC-201, Sigma). 20 million OCI-Ly7 cells were lysed in 800  $\mu$ L cold PURE Lysis Buffer containing 0.12% Triton X-100. The lysate was layered on 600  $\mu$ L of a 1.8 M sucrose cushion and centrifuged at 20000 g for 15 min at 4°C. The nuclear pellet was resuspended in 250  $\mu$ L cold glycerol buffer (20 mM Tris pH 7.9, 75 mM NaCl, 0.5 mM EDTA, 50% glycerol, 0.85 mM DTT) and then lysed with 250  $\mu$ L nuclear lysis buffer (20 mM HEPES pH 7.6, 7.5 mM MgCl<sub>2</sub>, 0.2 mM EDTA, 0.3 M NaCl, 1 M urea, 1% NP-40, 1 mM DTT). Chromatin was pelleted at 14000 g for 2 min at 4°C. RNase inhibitor (recombinant RNasin, N2511, Promega) was added to all buffers at 100 U/ml. RNA was isolated from the Chromatin-fraction using TRIzol reagent (Invitrogen).

Reads were mapped to hg38 using STAR v2.5 with default parameters. Bam files for each condition were merged with samtools v1.6. Merged bam files were converted to bigWigs using bamCoverage (deeptools v2.5). Separate bigWig files were generated for each strand.

### Transcription Factor Binding Motif Analysis

Binding motifs for OCT2 (MA0507.1) and MEF2B (MA0660.1) were downloaded from Jaspar 2018 using the R package TFBSTools v1.22. Edges with an information content < 0.5 were trimmed using the R package universalmotif v1.2.1. To search the *BCL6* locus for motif matches, motifs were converted to position weight matrices using a pseudocount of 0.8 (package universalmotif). For OCT2 motif density analysis, motif matches with a relative score > 0.8 ( $p < 0.005$ ) were considered.

### QUANTIFICATION AND STATISTICAL ANALYSIS

The two-sided t test was used unless otherwise stated. Statistical analyses were carried out using the R statistical package for Figures 2A, 3E, 5C, 5D, 5G, 5H, and 6. Statistical analyses were carried out using GraphPad Prism software for Figures 2G, 2H, 3, 4, 5E, and 5I–5K). Differences were considered significant with a p value of  $p < 0.05$ . P values are depicted in figures using one to three asterisks (\* $p < 0.05$ , \*\* $p < 0.01$ , and \*\*\* $p < 0.005$ ). Data are presented as  $\pm$  SEM with n indicating number of independent experiments if not stated otherwise in the figure legends or results.